

Structural basis for recognition and remodeling of the TBP:DNA:NC2 complex by Mot1

Agata Butryn¹, Jan M Schuller², Gabriele Stoehr¹, Petra Runge-Wollmann¹, Friedrich Förster², David T Auble^{3*}, Karl-Peter Hopfner^{1,4*}

¹Gene Center, Department of Biochemistry, Ludwig Maximilian University, Munich, Germany; ²Department of Molecular Structural Biology, Max Planck Institute of Biochemistry, Martinsried, Germany; ³Department of Biochemistry and Molecular Genetics, University of Virginia Health System, Charlottesville, United States; ⁴Center for Integrated Protein Sciences, Ludwig Maximilian University, Munich, Germany

Abstract Swi2/Snf2 ATPases remodel substrates such as nucleosomes and transcription complexes to control a wide range of DNA-associated processes, but detailed structural information on the ATP-dependent remodeling reactions is largely absent. The single subunit remodeler Mot1 (modifier of transcription 1) dissociates TATA box-binding protein (TBP):DNA complexes, offering a useful system to address the structural mechanisms of Swi2/Snf2 ATPases. Here, we report the crystal structure of the N-terminal domain of Mot1 in complex with TBP, DNA, and the transcription regulator negative cofactor 2 (NC2). Our data show that Mot1 reduces DNA:NC2 interactions and unbends DNA as compared to the TBP:DNA:NC2 state, suggesting that Mot1 primes TBP:NC2 displacement in an ATP-independent manner. Electron microscopy and cross-linking data suggest that the Swi2/Snf2 domain of Mot1 associates with the upstream DNA and the histone fold of NC2, thereby revealing parallels to some nucleosome remodelers. This study provides a structural framework for how a Swi2/Snf2 ATPase interacts with its substrate DNA:protein complex.

DOI: [10.7554/eLife.07432.001](https://doi.org/10.7554/eLife.07432.001)

*For correspondence: auble@virginia.edu (DTA); hopfner@genzentrum.lmu.de (K-PH).

Competing interests: The authors declare that no competing interests exist.

Funding: See page 18

Received: 11 March 2015

Accepted: 08 August 2015

Published: 10 August 2015

Reviewing editor: John Kuriyan, Howard Hughes Medical Institute, University of California, Berkeley, United States

 Copyright Butryn et al. This article is distributed under the terms of the [Creative Commons Attribution License](https://creativecommons.org/licenses/by/4.0/), which permits unrestricted use and redistribution provided that the original author and source are credited.

Introduction

Swi2/Snf2 (switch/sucrose non-fermenting 2) ATPases form a large and diverse class of proteins and multiprotein assemblies within the SF2 superfamily of helicases/translocases (Flaus et al., 2006). Swi2/Snf2 enzymes are best known as the principal catalytic subunits of large chromatin remodeling complexes that regulate the spatial arrangement and histone composition of nucleosomes, e.g. SWI/SNF, ISWI, CHD, and INO80 remodelers (Gangaraju and Bartholomew, 2007; Clapier and Cairns, 2009). Current models propose that Swi2/Snf2 ATPases track the minor groove of DNA, thereby generating tension that induces transient or permanent alterations in molecular assemblies (Saha et al., 2002; Whitehouse et al., 2003; Zofall et al., 2006). Although high-resolution structures of some Swi2/Snf2 domains and their substrate-interacting domains associated with DNA and protein have been previously described, detailed structural information about these ATPases bound to substrate proteins and DNA is largely absent (Dürr et al., 2005; Thomä et al., 2005; Shaw et al., 2008; Hauk et al., 2010; Sharma et al., 2011; Yamada et al., 2011). The lack of structural insights is owed to the complex, often multisubunit architecture of Swi2/Snf2 enzyme-containing complexes and their inherent structural flexibilities.

Mot1 (modifier of transcription 1, also denoted BTAF1) is conserved from protozoa to humans and was the first Swi2/Snf2 member for which the biochemical activity has been demonstrated in vitro (Auble and Hahn, 1993). Mot1 dissociates TATA box-binding protein (TBP) from DNA in an ATP-dependent manner,

eLife digest An organism's DNA contains thousands of genes, not all of which are active at the same time. Cells use a number of methods to carefully control when particular genes are switched on or off. For example, proteins called transcription factors can activate a gene by binding to particular regions of DNA called promoters. One such transcription factor is called the TATA-binding protein (TBP for short). Mot1 is a remodeling enzyme that can form a "complex" with TBP by binding to it, and in doing so remove TBP from DNA. This silences the genes at those sites. The freed TBP can then bind to other promoters that lack Mot1 and activate the genes found there.

In 2011, researchers revealed the structure of the complex formed between TBP and Mot1 after TBP has been detached from DNA. However, the structure of the complex that forms while TBP is still bound to the DNA molecule was not known. Butryn et al. – including several of the researchers involved in the 2011 work – have now described the structure of this complex using X-ray crystallography and electron microscopy. Another protein called negative cofactor 2 is also part of the complex, and helps to stabilize it.

Butryn et al. found that Mot1 reduces the strength of the interactions between DNA and both TBP and negative cofactor 2. Binding to TBP and negative cofactor 2 causes the DNA molecule to bend; however, if Mot1 is also in the complex, the DNA becomes less bent. By making these changes, Mot1 is likely to prime TBP to detach from the DNA. Since the current structures do not yet reveal the atomic structure of Mot1's ATP dependent DNA motor domain, the next challenge is to visualize the entire complex at atomic resolution.

DOI: [10.7554/eLife.07432.002](https://doi.org/10.7554/eLife.07432.002)

thereby directly regulating transcription initiation process and global redistribution of TBP in the cell (Auble and Hahn, 1993; Dasgupta et al., 2002; Darst et al., 2003; Zentner and Henikoff, 2013). In contrast to the majority of other Swi2/Snf2 enzymes, Mot1 does not require any associated subunit for its essential activity and serves as a useful model system for studying Swi2/Snf2 enzymes in vitro. The crystal structure of the N-terminal domain of *Encephalitozoon cuniculi* Mot1 (Mot1^{NTD}) in complex with TBP showed that Mot1 consists of 16 HEAT repeats (Huntingtin, elongation factor 3, protein phosphatase 2A, lipid kinase TOR) that are arranged in a horseshoe-like shape (Wollmann et al., 2011). Of note was that a long loop between HEAT repeats 2 and 3, denoted as the 'latch', can bind to TBP's concave site and block TBP-DNA association. Therefore, previous analyses have revealed not only how Mot1 binds TBP, but also that Mot1 functions as a TBP chaperone. Numerous biochemical and more recent structural studies of the Mot1:TBP complex predicted the approximate positioning of the ATPase domain (Mot1^{CTD}) with respect to the DNA upstream of the TATA box (Auble and Hahn, 1993; Auble et al., 1994; Darst et al., 2001; Gumbs et al., 2003; Sprouse et al., 2006; Wollmann et al., 2011; Moyle-Heyrman et al., 2012). A limitation of our previous work on Mot1:TBP was the finding that the crystallized state evidently represents the 'product' state after the remodeling reaction took place, but it remained unclear how Mot1 directly impacts the TBP:DNA 'substrate' state prior to the remodeling reaction (Wollmann et al., 2011). Obtaining a substrate state with DNA and TBP turned out to be difficult because Mot1^{NTD} can disrupt TBP:DNA by its latch. However, we found that the Mot1:TBP:DNA complex is much more stable in the presence of negative cofactor 2 (NC2), another global transcriptional regulator, whose occurrence coincides with Mot1 and TBP at many genomic locations (Andrau et al., 2002; Dasgupta et al., 2002; Hsu et al., 2008; Van Werven et al., 2008; Spedale et al., 2012). NC2 is a heterodimer composed of α and β subunits, which highly resemble histones H2A and H2B, respectively (Kamada et al., 2001). We crystallized *E. cuniculi* Mot1^{NTD} in complex with TBP, NC2, and a TATA promoter DNA fragment and present here the crystal structure of this complex at 3.8 Å resolution along with biochemical, electron microscopy, and cross-linking studies of the full-length Mot1 complex. Our study provides the first pseudoatomic view of a Swi2/Snf2 ATPase in complex with a DNA:protein substrate complex.

Results

Mot1, TBP, and NC2 form a stable complex on promoter DNA in vitro

Previous studies found that *Saccharomyces cerevisiae* Mot1 and NC2 can simultaneously bind to the TBP:DNA complex and could be isolated as a complex from yeast extracts (Darst et al., 2003;

Van Werven et al., 2008), suggesting that TBP:NC2 is a physiological substrate for Mot1. In contrast, human NC2 was reported to replace the human Mot1 homolog BTAF1 bound to TBP:DNA complexes (*Klejman et al., 2004*). These observations prompted us to explore whether *E. cucuruli* Mot1, TBP, NC2 α , and NC2 β form a stable complex with DNA in vitro. In line with the results demonstrated in the *S. cerevisiae* system (*Darst et al., 2003; Van Werven et al., 2008*), we were able to reconstitute the Mot1:TBP:NC2 α :NC2 β complex in the presence of a TATA box consensus sequence-containing oligonucleotide and to purify it by gel filtration (**Figure 1**). The Mot1^{NTD} also formed a stable complex with TBP, NC2, and DNA (**Figure 1—figure supplement 1**). From these data, it appears that complex formation between Mot1, TBP, and NC2 on TATA DNA is evolutionary conserved. Furthermore, specific interactions between Mot1 and TBP—and not for instance interactions between the Mot1^{CTD} and the DNA—are sufficient for formation of the pentameric complex.

Mot1 dissociates the TBP:DNA:NC2 complex in the presence of ATP

Having found that NC2 stabilized the Mot1:TBP:DNA:NC2 complex, we tested if Mot1 had the ability to dissociate the TBP:DNA:NC2 complex. Consistent with the studies performed on the yeast proteins (*Darst et al., 2003; Van Werven et al., 2008*), *E. cucuruli* Mot1 efficiently disrupted the TBP:DNA:NC2 complex in an ATP-dependent manner

(**Figure 2A**). The latch was important for this process in reactions both with and without NC2 (**Figure 2A**). Of note is that the presence of the NC2 subunits substantially increased the stability of the Mot1^{NTD}:TBP:DNA complex and limited Mot1^{NTD}'s ability to disrupt TBP:DNA with its 'latch' competitor (**Figure 2B**). However, we were not able to detect any significant changes in the Mot1-catalyzed TBP:DNA dissociation rate or the ATP hydrolysis rate of this process in the presence of NC2 (**Figure 3**). Taken together, these data show that the TBP:DNA:NC2 complex is a bona fide substrate of Mot1's remodeling activity. Moreover, in contrast to the TBP:DNA substrates, the ATPase domain is necessary to disrupt the NC2-containing complexes.

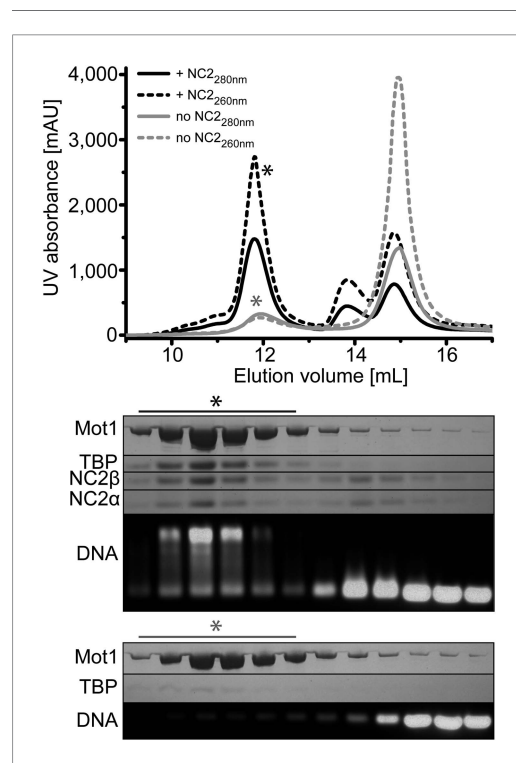


Figure 1. Size exclusion chromatography of the *E. cucuruli* Mot1:TBP:DNA:NC2 complex. Upper panel: elution profiles of Mot1:TBP:DNA complex (gray) and Mot1:TBP:DNA:NC2 complex (black). Absorbance at 260 nm is represented by dashed lines and at 280 nm as solid lines. Lower panel: analysis by SDS-PAGE (Coomassie staining) and agarose gel electrophoresis (Gel-Red staining). The asterisk marks fractions containing all components. DOI: [10.7554/eLife.07432.003](https://doi.org/10.7554/eLife.07432.003)

The following figure supplement is available for figure 1:

Figure supplement 1. Size exclusion chromatography of the *E. cucuruli* Mot1^{NTD}:TBP:DNA:NC2 complex. DOI: [10.7554/eLife.07432.004](https://doi.org/10.7554/eLife.07432.004)

Organization of the Mot1^{NTD}:TBP:DNA:NC2 complex reveals a high level of structural conservation

Our previously reported Mot1^{NTD}:TBP complex structure likely represents the 'product' state of Mot1's remodeling reaction, i.e., after TBP has been dissociated from DNA (*Wollmann et al., 2011*). To capture how Mot1 binds its 'substrate' TBP:DNA complex, i.e., the interaction that is formed before the remodeling reaction takes place, we performed extensive crystallization experiments. Owing to the inherent instability of the Mot1^{NTD}:TBP:DNA complex, we obtained only Mot1^{NTD}:TBP crystals. However, the addition of NC2 efficiently stabilized the 'substrate' complex and we obtained crystals from selenomethionine-derivatized proteins diffracting to 3.8 Å resolution that contained all five components: Mot1^{NTD}, TBP, NC2 α , NC2 β , and 24 base-paired TATA box-containing DNA. The structure was solved by

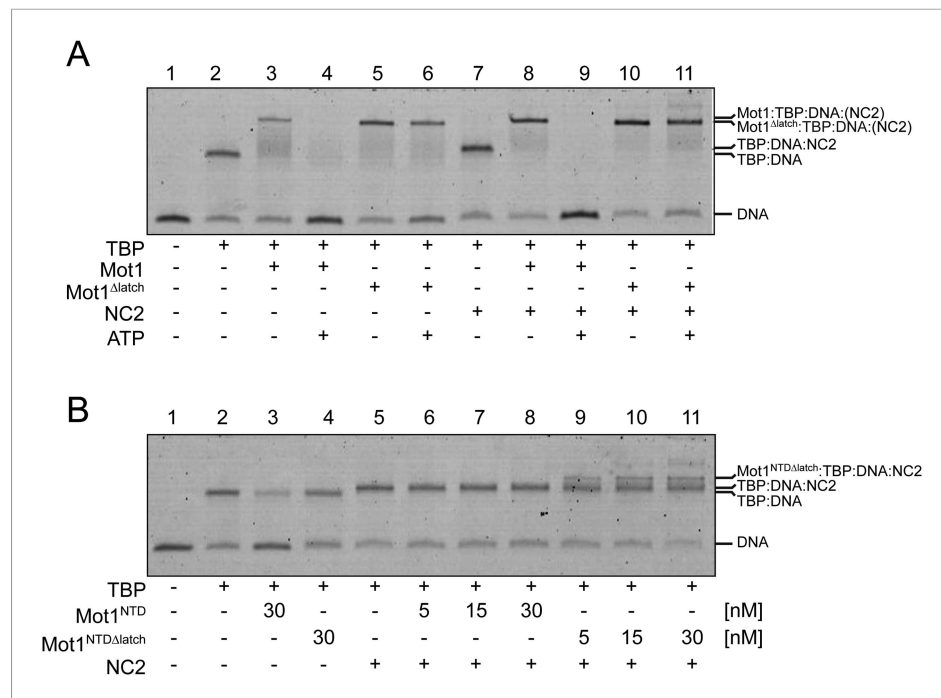


Figure 2. Electrophoretic mobility shift analysis of Mot1:TBP:DNA:NC2 complexes. **(A)** Upon ATP addition, Mot1 dissociated TBP from DNA (lanes 3 and 4) as well as the TBP:DNA:NC2 complex (lanes 8 and 9). Mot1^{Δlatch} was impaired in TBP removal (lanes 5 vs 6 and 10 vs 11). **(B)** Effect of NC2 on ATP-independent remodeling by Mot1^{NTD}. Addition of NC2 prevented the Mot1^{NTD} from displacing TBP from DNA (lane 3 and 6–8). The Mot1^{NTDΔlatch} protein bound TBP:DNA more stably than Mot1^{NTD} (lane 4). Addition of NC2 to Mot1^{NTDΔlatch}:TBP:DNA complex resulted in a distinct shift (lanes 9–11), consistent with formation of a stable complex containing all components.

DOI: 10.7554/eLife.07432.005

molecular replacement using *E. cuculii* Mot1^{NTD} and TBP (Wollmann et al., 2011) as the search models. The initial fragments of DNA and NC2—based on the human TBP:DNA:NC2 (Kamada et al., 2001) and NF-Y complex (Nardini et al., 2013)—were manually fitted according to the difference density, refined as rigid bodies, and extended. We used the feature-enhanced $2F_o - F_c$ maps implemented in PHENIX to reduce the model bias and to enable unambiguous density interpretation (Afonine et al., 2015). The final model was refined to R_{work}/R_{free} of 23.5/25.8% with good stereochemistry (Table 1) and includes 39 out of the 48 DNA bases as well as 89% of all protein residues. The sequence register was confirmed by computing anomalous difference density map that showed signal of the selenium atoms (Figure 4—figure supplement 1B).

In the crystal structure, we find one copy each of Mot1^{NTD}, TBP, NC2 α , NC2 β , and 24 base pairs of DNA, in a semi-compact complex with approximate dimensions of 100 Å × 95 Å × 95 Å (Figure 4). Mot1 and NC2 occupy opposite binding surfaces on TBP and completely encircle the DNA-bound TBP molecule, which recognizes the minor groove of the TATA sequence. The Mot1^{NTD} is oriented towards the upstream DNA (the 5' end of the TATA box-containing strand) and predominantly binds the convex ('top') side of TBP. Furthermore, like in the human TBP:DNA:NC2 complex, NC2 locks TBP onto the promoter utilizing its histone fold domain (NC2^{HF}), which is bound to the underside of the DNA, and the C-terminal helix H5 of NC2 β , which reaches around the DNA and binds the convex side of TBP (Kamada et al., 2001). Of note is that no interpretable electron density of the Mot1 latch residues 98–142 is observed. Therefore, it is probable that the latch is ordered only after binding to TBP's DNA-binding surface. Taken together, the *E. cuculii* Mot1^{NTD}:TBP:DNA:NC2 crystal structure shows a high degree of evolutionary conservation of the TBP:NC2 interaction on a structural level. Moreover, the encircling of TBP:DNA by NC2 explains the resistance of Mot1^{NTD}:TBP:DNA:NC2 complex to premature dissociation caused by the latch.

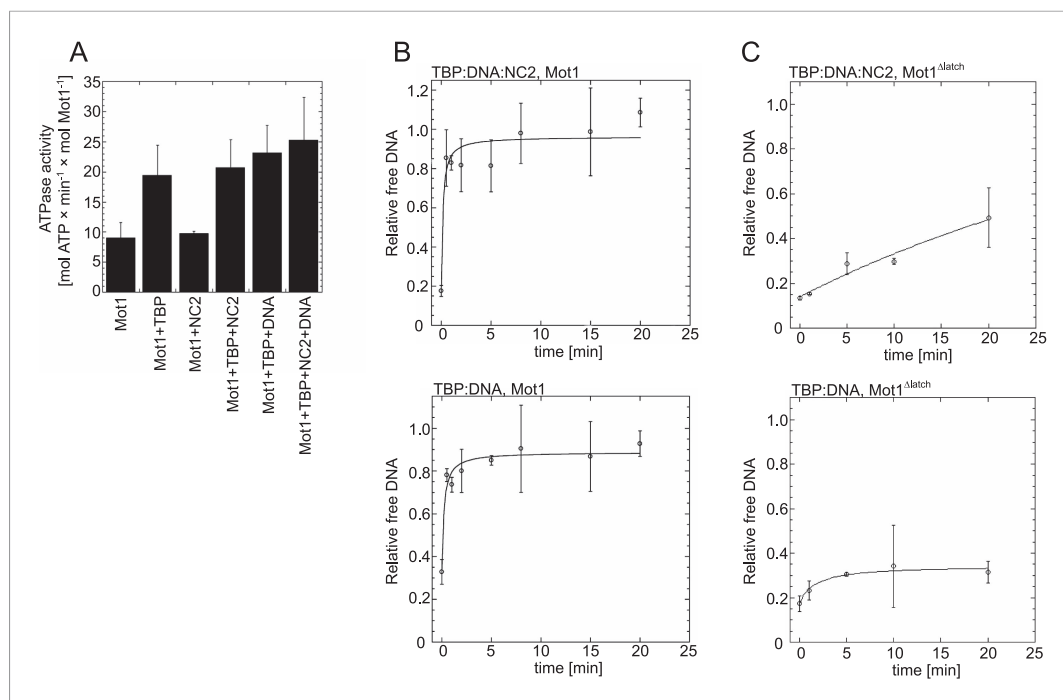


Figure 3. Effect of NC2, TBP, and DNA on Mot1's activity. **(A)** The graph shows the steady-state ATPase activity of 8 nM Mot1 alone or in the presence of 80 nM NC2 and/or TBP and with or without 23 nM TATA-containing DNA. The assays were performed as described previously (Wollmann *et al.*, 2011). The data represent the mean \pm the standard deviation obtained from at least two independent experiments. **(B)** The graphs show the rates of Mot1-catalyzed TBP:DNA:NC2 dissociation (top) and TBP:DNA dissociation (bottom) measured by quantitation of the free DNA level by EMSA following ATP addition to pre-formed complexes. The assays were performed as previously described (Wollmann *et al.*, 2011). **(C)** The same as in **(B)** shown for the Mot1^{Δlatch} mutant. DOI: 10.7554/eLife.07432.006

Mot1 binding induces changes in the interaction interfaces in the 'substrate' complex

The Mot1-bound 'substrate' state superficially appears to be a superposition of the Mot1^{NTD}:TBP 'product' state and the TBP:DNA:NC2 'substrate' complex, with the important exception that the latch in the DNA-bound complex is displaced (Figure 5A). Although the contacts of Mot1^{NTD} and NC2 within the complex are mainly TBP- and/or DNA-mediated, which is consistent with the lack of a stable interaction between Mot1 and NC2 in the absence of DNA *in vitro* (data not shown), we observed several notable conformational differences. In comparison with the Mot1^{NTD}:TBP 'product' state, the interaction between the Mot1^{NTD} and the convex site of TBP prominently extends towards the C-terminus of Mot1^{NTD}, engaging HEAT repeats 4 to 10 and the insertion domain. Additionally, the 'anchor' helix H5 of NC2β bound to the upper side of TBP contacts the insertion domain of Mot1^{NTD}, the only non-HEAT repeat stretch in the N-terminal part of Mot1 (Figure 5B and Figure 5—figure supplement 1A). As a result, the interaction interface between Mot1^{NTD} and TBP's convex surface increases dramatically from $\sim 900 \text{ \AA}^2$ to $\sim 1500 \text{ \AA}^2$, as calculated using the PISA server (Krissinel and Henrick, 2007), thus suggesting that Mot1 might even have a tighter grip on TBP in the presence of NC2. The additional interactions between the loops and structural elements of the Mot1^{NTD} and TBP result in a considerable compaction of the α -helical HEAT repeat array. Therefore, since the capability to rearrange was shown to be an essential property of long α -helical solenoids, shape adaptation and conformational changes of the Mot1's HEAT domain might play an important role in the dissociation mechanism (Grünwald *et al.*, 2013).

Interestingly, the kink of the longitudinal axis of the DNA duplex introduced by TBP appears to be less severe than the $\sim 90^\circ$ bend observed in other TBP:DNA complexes and is slightly underwound (Figure 5C and Figure 5—figure supplement 1B) bringing the upstream DNA closer to the N- and

Table 1. Data collection and refinement statistics
Data collection*

Space group	C 1 2 1
Cell dimensions	
a, b, c (Å)	150.6, 140.3, 90.8
α, β, γ (°)	90.0, 113.7, 90.0
Resolution (Å)	49.2–3.8 (4.0–3.8)†
R_{merge} (%)	10.4 (78.9)
$CC_{(1/2)}$	99.8 (83.8)
$I/\sigma I$	7.5 (1.5)
Completeness (%)	98.2 (93.5)
Redundancy	3.4 (3.4)
Refinement	
Resolution (Å)	49.2–3.0 (4.0–3.8)
No. reflections	17,163
$R_{\text{work}}/R_{\text{free}}$ (%)	23.5/25.8 (26.9/30.2)
No. atoms	
Protein	8422
DNA	799
Ligand/ion	0
Water	0
Isotropic B-factors (Å ²)	
Protein	69
DNA	135
R.m.s. deviations	
Bond lengths (Å)	0.009
Bond angles (°)	0.75

*From one crystal.

†Values in parentheses are for the highest-resolution shell.

DOI: [10.7554/eLife.07432.007](https://doi.org/10.7554/eLife.07432.007)

C-termini of Mot1^{NTD} (the ‘gap’ of the horseshoe, **Figure 5—figure supplement 1C**). This observation is of potential importance since the upstream part of DNA binds to the Mot1’s Swi2/Snf2 domain, which immediately follows the C-terminus of Mot1^{NTD} (**Auble and Hahn, 1993; Auble et al., 1994; Sprouse et al., 2006; Darst et al., 2001; Wollmann et al., 2011**). Furthermore, the linker helix H4 of NC2 β adopts a partially unfolded conformation and its interaction with the major groove of the downstream DNA is lost (**Figure 5D**). Thus, Mot1 might influence the C-terminal stirrup of TBP indirectly via interaction with NC2. (**Figure 5—figure supplement 1B**). Moreover, due to the changed DNA geometry, NC2^{HF} is moved and rotated with respect to TBP. Despite this change, the direct interaction between the NC2^{HF} and DNA does not seem to be affected and is similar to the interaction of histones H2A/H2B with DNA in the nucleosome (**Luger et al., 1997**). However, it has to be noted that both sides of the DNA molecule are engaged in the formation of crystal contacts; thereby, we cannot exclude the possibility that the DNA conformation is affected by crystal packing. Nevertheless, it is unlikely that crystal lattice formation can entirely explain the change in DNA trajectory (see ‘Discussion’). In summary, in the Mot1^{NTD}:TBP:DNA:NC2 complex crystal structure, we observe a variety of small to medium conformational changes. The observed changes indicate reduced strength of the TBP–DNA and DNA–NC2 interactions as well as stabilization of Mot1–TBP interface due to Mot1^{NTD} binding.

In the presence of ATP analogs Mot1 ATPase domain adopts a ‘closed’ conformation

Upstream DNA was shown to play a crucial role not only in the stabilization of Mot1:TBP:DNA complexes, but also in the ATP-mediated dissociation in vitro (**Auble and Hahn, 1993; Darst et al., 2001; Gumbs et al., 2003; Sprouse et al., 2006; Moyle-Heyrman et al., 2012**). Additionally, it is known that the nucleotide state of Swi2/Snf2 domains modulates their conformation and affinity for DNA (**Lewis et al., 2008; Moyle-Heyrman et al., 2012**). Therefore, in order to define the location of the Swi2/Snf2 domain in the Mot1:TBP:DNA:NC2 complex, we analyzed the full-length complex by chemical cross-linking combined with mass spectrometry (CX-MS) as well as by negative stain electron microscopy (EM, see below).

To facilitate this analysis, we formed the Mot1:TBP:DNA:NC2 complex on long TATA box-containing DNA (at least 26 base pairs upstream from the TATA box) and used ADP·BeF_x, ATP γ S, and ADP to lock the ATPase domain in ATP- and ADP-bound states (**Ponomarev et al., 1995**). In our analysis, we identified 133, 129, and 97 inter- and intra-protein cross-links within the ADP·BeF_x-, ATP γ S- and ADP-bound Mot1:TBP:DNA:NC2 complexes, originating from 116, 109, and 82 non-redundant lysine linkage pairs, respectively (**Figure 6—figure supplement 1, Table 2 and Table 2—source data 1**). Most of the cross-links could be placed within the crystal structure or within the Mot1^{CTD}. The cross-links that were detected between the latch (Lys115 or Lys138) and other components could not be mapped since the latch is disordered in the crystal structure. The latch

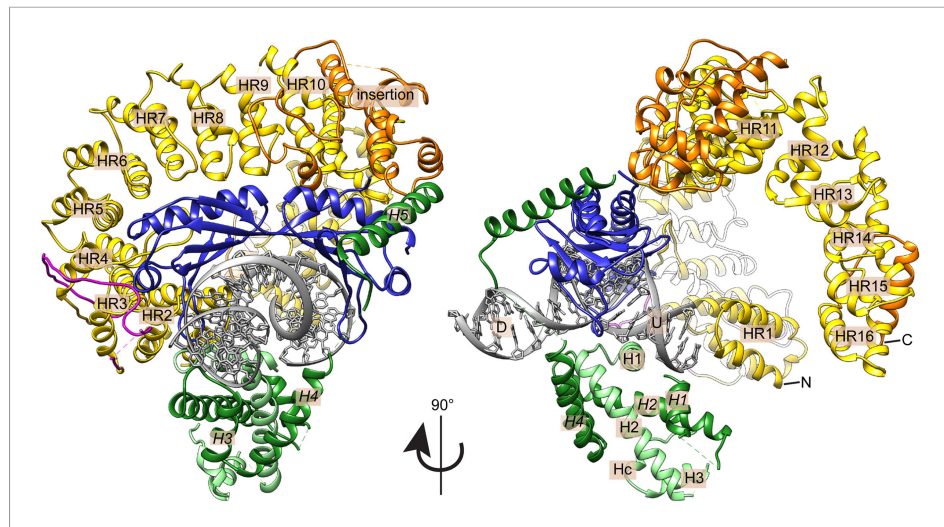


Figure 4. Crystal structure of the *E. cuniculi* Mot1^{NTD}:TBP:DNA:NC2 complex. Front and side views of the structure, represented as cartoon models with highlighted secondary structure. TBP (blue), NC2 α (light green), and NC2 β (dark green) encircle kinked promoter DNA (gray with upstream (U) and downstream (D) regions labeled). The HEAT repeats (HR, yellow with N- and C-termini marked) and insertion domain (orange) of the Mot1^{NTD} bind along the convex surface of TBP and contact the C-terminal helix (H5) of NC2 β . The latch of Mot1^{NTD} (magenta), which has been previously shown to bind to TBP's DNA-binding cleft, is mostly disordered in the presence of DNA and NC2. DOI: [10.7554/eLife.07432.008](https://doi.org/10.7554/eLife.07432.008)

The following figure supplement is available for figure 4:

Figure supplement 1. X-ray electron density maps.

DOI: [10.7554/eLife.07432.009](https://doi.org/10.7554/eLife.07432.009)

formed contacts with TBP, Mot1^{CTD} as well as NC2^{HF}, consistent with its high flexibility even in the context of full-length Mot1. The remaining cross-links were detected between Mot1^{CTD} and the rest of the complex. As an example, in all data sets, we found numerous cross-links between the Mot1^{CTD} and NC2^{HF}, mainly between the helix Hc and loop L2 (joining helices H3 and Hc) of NC2 α and RecA2 subdomain of Mot1^{CTD} (**Figure 6A**).

As shown in **Figure 6B**, in the crystal structures of Swi2/Snf2 ATPase domains, the two RecA-fold subdomains were observed to adopt a variety of different positions with respect to each other, ranging from 'open' and 'semi-closed' to 'closed' (**Dürr et al., 2005; Thomä et al., 2005; Shaw et al., 2008; Hauk et al., 2010**). Importantly, on the basis of related SF2 helicases, ATP was shown to bind to the interface of the RecA-fold subdomains and stabilize a 'closed' state (**Sengoku et al., 2006**). The CX-MS approach can provide insights into the architecture of protein complexes with domain to motif resolution (**Nguyen et al., 2013; Tosi et al., 2013; Politis et al., 2014**). Therefore, to gain insights into the conformation of the Swi2/Snf2 domain in different nucleotide states, we analyzed the 32 cross-links that we detected between the two RecA-fold subdomains within Mot1^{CTD} and mapped them onto homology models of Mot1^{CTD} in different conformations, based on 'open', 'semi-closed' and 'closed' states. Among these cross-links, 18 do not distinguish between these conformations, since they are all either below (14) or above (4) the distance cutoff of 30 Å, which accounts for the length of the cross-linker and two lysine side chains (**Politis et al., 2014, Table 3** part A). From the cross-links, which do distinguish between the conformations, two were present in all three data sets (ADP, ATP γ S, ADP·BeF_x) and are thus non-informative (**Table 3** part B). However, the remaining 4 cross-link sites (8 cross-links total) were detected only in the presence of ADP·BeF_x and ATP γ S (**Table 3** part C). Notably, all of these cross-links, which were absent from the ADP data set, are only consistent with the 'closed' conformation (**Figure 6C, Figure 6—figure supplement 2**). Thus, our data suggest that the ATP-mimicking ADP·BeF_x and ATP γ S analogs stabilize a more 'closed' conformation. Since we did not detect any cross-links that would be unique for the ADP-supplied sample, whether Mot1^{CTD} adopts a distinct state in the presence of this nucleotide or is simply more flexible remains to be addressed in future studies.

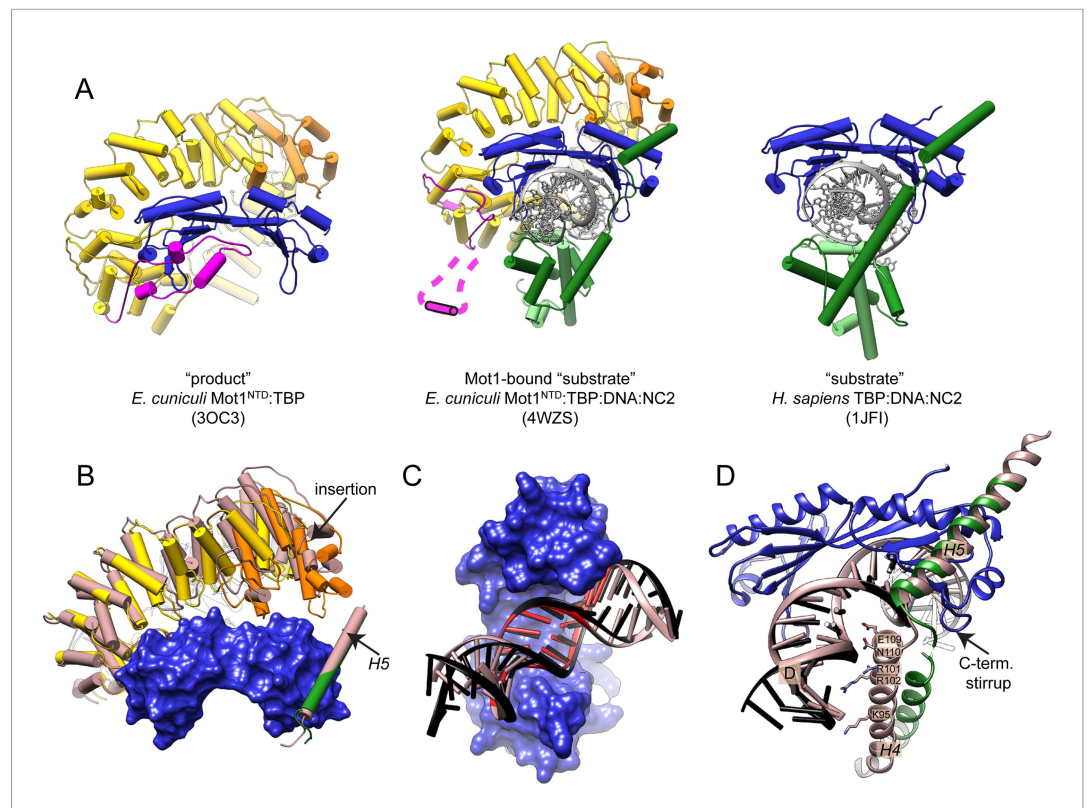


Figure 5. Features of the Mot1-bound 'substrate' complex. **(A)** Comparison of the 'product' (left, *Wollmann et al., 2011*), 'substrate' (right, *Kamada et al., 2001*), and Mot1-bound 'substrate' complex (center). Mot1's latch in the latter structure is disordered and represented schematically. Color code is as in *Figure 4*. Panel **(B)** shows Mot1^{NTD} and TBP from the Mot1^{NTD}:TBP:DNA:NC2 structure (color code as in *Figure 4*) superimposed via TBP with the 'product' Mot1^{NTD}:TBP structure and NC2 β H5 from the 'substrate' TBP:DNA:NC2 structure (both shown in light brown). Mot1^{NTD} shifts toward H5 and TBP although the position of H5 is not affected. Panels **(C)** and **(D)** show conformational changes of NC2 and DNA in the Mot1^{NTD}:TBP:DNA:NC2 complex structure (color code as in *Figure 4*) compared to the TBP:DNA:NC2 'substrate' complex (shown in light brown) superimposed via TBP. **(C)** View from the concave side of TBP shows that in the presence of Mot1, DNA is partially straightened and underwound. TATA box region is highlighted in red. Panel **(D)** shows that partially unfolded helix H4 of NC2 β , which joins the NC2^{HF} with helix H5, loses its interaction with downstream DNA and is close to TBP's C-terminal stirrup. DOI: [10.7554/eLife.07432.010](https://doi.org/10.7554/eLife.07432.010)

The following figure supplement is available for figure 5:

Figure supplement 1. Mot1^{NTD}:TBP:DNA:NC2 structure features. DOI: [10.7554/eLife.07432.011](https://doi.org/10.7554/eLife.07432.011)

EM and CX-MS provide important insights into Mot1^{CTD} localization and orientation

We next visualized the Mot1:TBP:DNA:NC2 complex by electron microscopy. We calculated a negative stain reconstruction of the Mot1:TBP:DNA:NC2 complex in the presence of ADP·BeF_x and experimentally determined its handedness (*Figure 7—figure supplement 1*). The 22 Å reconstruction, of overall dimensions of 115 Å × 115 Å × 100 Å, is in good agreement with the size of the partial complex observed in the crystal structure. Due to better resolution, the characteristic 'C'-shaped structure of Mot1^{NTD} is more pronounced than in the reconstruction of the *E. cuniculi* Mot1:TBP and *H. sapiens* BTA1:TBP complexes (*Pereira et al., 2004; Wollmann et al., 2011*). Furthermore, to place the Mot1^{NTD}:TBP:DNA:NC2 crystal structure model into the EM density, we employed an unsupervised rigid body docking approach using the *Situs* software package (*Wriggers, 2010*), which resulted in a convincing solution (*Figure 7A*). The prominent and centered additional density, which is localized in the immediate vicinity of the N- and C-terminal ends of Mot1^{NTD}

Table 2. Localization of the cross-links identified in Mot1:TBP:DNA:NC2 complex

Experiment	Crystal structure	Within Mot1 ^{CTD}		Latch-crystal		Crystal structure– Mot1 ^{CTD}	Total	Decoy§	Estimated FDR [%]
		Intralobe*	Interlobe [†]	structure	Latch– Mot1 ^{CTD}				
ADP-BeF _x	46 (42)	21 (17)	15 (12)	8 (8)	5 (5)	37 (31) + 1 (1)‡	133 (116)	2	0.8
ATPγS	51 (44)	17 (14)	10 (9)	11 (11)	3 (3)	37 (28)	129 (109)	1	1.5
ADP	40 (36)	14 (11)	7 (7)	11 (10)	4 (3)	21 (15)	97 (82)	2	2.0

*Within RecA1 or RecA2 subdomain.

†Between RecA1 and RecA2 subdomain.

‡Between Mot1^{CTD} and the linker joining N- and C-terminal domains (could not be mapped).

§Detected from a reverse database, estimating false-discovery rate.

Numbers refer to the total number of cross links, including cross-linked sites which were detected more than once (i.e., from miss-cleaved peptides).

Numbers in brackets refer to non-redundant linkages only.

DOI: [10.7554/eLife.07432.012](https://doi.org/10.7554/eLife.07432.012)

Source data 1. Full list of the detected cross-links.

DOI: [10.7554/eLife.07432.013](https://doi.org/10.7554/eLife.07432.013)

(the ‘gap’ of the horseshoe), likely harbors the C-terminal Swi2/Snf2 domain (**Figure 7B**). To assess the placement of Mot1^{CTD}, we again used our CX-MS data. Using RANCH (**Petoukhov et al., 2012**), we first generated a set of 20,000 theoretical Mot1:TBP:DNA:NC2 assemblies allowing flexible movement of the eight amino acid linker joining the Mot1^{CTD} model and Mot1^{NTD}. As suggested by the interpretation of the CX-MS data, for this analysis we used the Mot1^{CTD} modeled in the ‘closed’ conformation. On each of the computed models, we next mapped all of the non-redundant cross-links between Mot1^{CTD} and the rest of the complex. We repeated this procedure for the ATPγS and ADP-BeF_x data sets independently (using 28 and 31 cross-links, respectively). We then performed violation scoring by applying the 30 Å cutoff distance. Convincingly, for both of the independently analyzed data sets exactly the same models were among best-scored ensembles (the lowest violation scores, **Figure 7—figure supplement 2**).

The EM- and CX-MS-derived placements not only converged, but are also in excellent agreement with the localization that has been previously determined in biochemical assays (**Auble and Hahn, 1993; Auble et al., 1994; Darst et al., 2001; Gumbs et al., 2003; Sprouse et al., 2006; Wollmann et al., 2011; Moyle-Heyrman et al., 2012**). In such an arrangement, the upstream DNA engaged by Mot1^{CTD} directly continues from the upstream DNA of the Mot1^{NTD}:TBP:DNA:NC2 complex (**Figure 7C,D**). Accounting for slight rearrangements within the HEAT repeats, the analysis implies that Mot1^{CTD} would contact DNA not further than ~20 bp upstream from the TATA sequence. This would be in agreement with the requirement reported for the yeast Mot1, which was shown to contact around 17 bp upstream from the TATA box (**Wollmann et al., 2011**). It is, however, not clear if the upstream NC2-bound DNA adopts B-DNA form or, like in case of a related histone fold transcriptional factor NF-Y, has bent, nucleosome-like curvature (**Huber et al., 2012; Nardini et al., 2013**).

Mot1 locally dissociates the TBP:DNA:NC2 complex

Swi2/Snf2 ATPase motors couple ATP hydrolysis to translocation along dsDNA (**Saha et al., 2002; Whitehouse et al., 2003; Zofall et al., 2006**). The release of TBP from DNA by Mot1, however, does not appear to involve highly processive ATP-dependent DNA tracking (**Auble and Steggerda, 1999**). The changes in the TBP:DNA and NC2:DNA interactions observed in the Mot1^{NTD}:TBP:DNA:NC2 crystal structure suggest that Mot1^{NTD} binding leads to an alteration of the interaction with promoter DNA. Such a potential destabilization—due to the ring that is formed around DNA by TBP and NC2—does not generally result in removal from TBP from DNA, consistent with our biochemical observations. However, it is possible that TBP:NC2 has an increased lateral mobility on DNA. Interestingly, in single-molecule experiments, NC2 induces dynamic conformational changes in the TBP:DNA interface, enabling TBP to laterally move on DNA substrates (**Schluesche et al., 2007**). Consequently, NC2-induced lateral mobility of TBP was proposed to explain how NC2, by sliding TBP, could lead to TBP repositioning from/towards the promoter sites. Although the underlying conformational changes have not been seen in the TBP:DNA:NC2 crystal structure, our structural

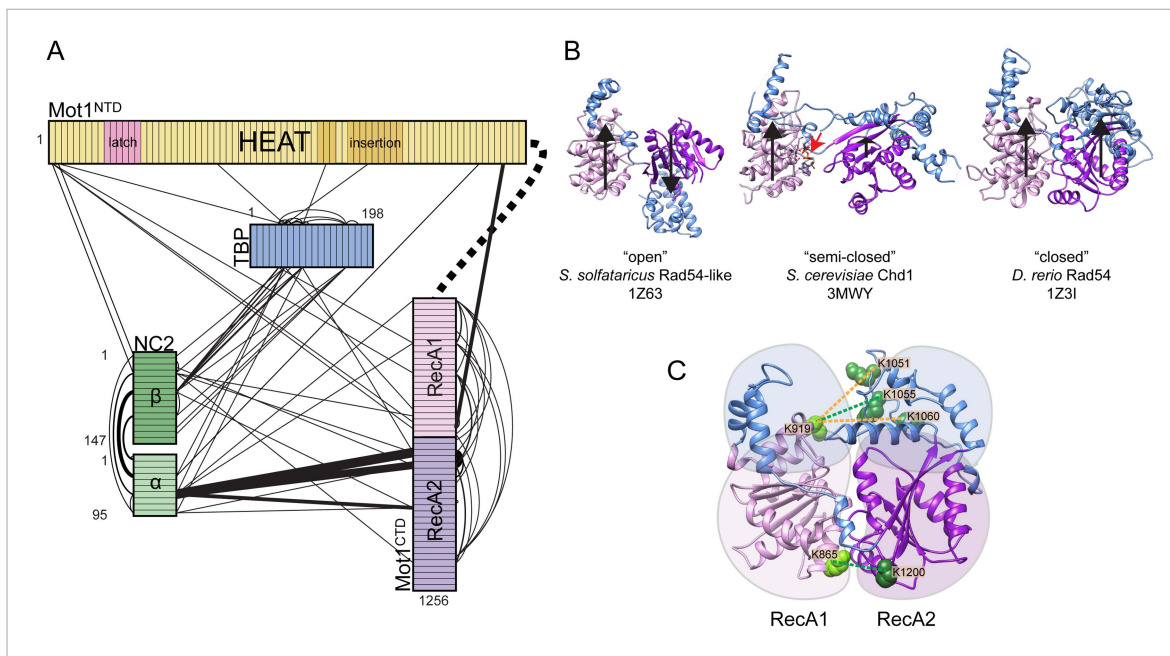


Figure 6. Mot1:TBP:DNA:NC2 complex analyzed by CX-MS. **(A)** General topology of the Mot1:TBP:DNA:NC2 complex in the presence of ATP γ S derived from the CX-MS data. Each polypeptide is divided into 10 amino acid segments. The black solid lines represent the identified cross-links. For simplicity, cross-links to the latch region of Mot1 are not displayed. Line thickness is proportional to the number of cross-links detected between joined segments. The dashed line between Mot1^{NTD} and Mot1^{CTD} represents the eight amino acid linker between these domains. **(B)** Crystal structures of Swi2/Snf2 domains used for the cross-link analysis: *Sulfolobus solfataricus* Rad54-like in an 'open' conformation (Dürr et al., 2005), *Saccharomyces cerevisiae* Chd1 in a 'semi-closed' conformation (Hauk et al., 2010) in the presence of ATP γ S (red arrow) and *Danio rerio* Rad54 in a 'closed' conformation (Thomä et al., 2005). PDB accession codes are included. The structures are oriented with respect to the RecA1 subdomain. Relative orientations of the RecA1 (pink) and RecA2 (purple) subdomains are represented by the black arrows. Family-specific insertion regions are indicated in blue. Auxiliary domains were omitted. Panel **(C)** shows cross-linked sites listed in **Table 3** part C mapped on the Swi2/Snf2 domain modeled in the 'closed' conformation. Cross-links detected only in the presence of ADP·BeF_x and ATP γ S are shown as green dashed lines, whereas the cross-links present only in the ADP·BeF_x data set are in orange. DOI: 10.7554/eLife.07432.014

The following figure supplements are available for figure 6:

Figure supplement 1. Titration of the cross-linking agent disulfosuccinimidyl glutarate (DSSG).

DOI: 10.7554/eLife.07432.015

Figure supplement 2. Analysis of the cross-links between RecA1 and RecA2 subdomains within the Mot1^{CTD} models.

DOI: 10.7554/eLife.07432.016

analysis indeed indicates changes in the DNA trajectory that are consistent with increased lateral mobility. Thus, the analysis of our structural data suggested two models for the observed dissociation of the Mot1:TBP:DNA:NC2 complex in the presence of ATP. One possibility is that Mot1 uses a Swi2/Snf2 translocase activity to translocate the TBP:NC2 ring along DNA like a sliding clamp without disrupting it. In our EMSAs, the complex would eventually dissociate from DNA when the DNA end is reached. Alternatively, Mot1-induced conformational changes in the TBP:DNA:NC2 substrate could directly dissociate the complex from DNA without translocation along the DNA. To distinguish between these two options, we performed EMSAs using digoxigenin-labeled DNA, the ends of which were blocked with an anti-digoxigenin antibody. The DNA probes used were not much longer than the minimal DNA required for the formation of the complex, consisting of just 30 bp of DNA upstream of the TATA box and 9 bp of DNA downstream. As shown in **Figure 8**, we observed no significant impact of the presence or placement of antibody block on either side of the DNA on the efficiency of the remodeling reaction. Therefore, in this setting Mot1 does not appear to apply highly processive sliding of TBP:NC2 along DNA but rather utilizes a more direct, local disruption mechanism consistent with previous studies of TBP–DNA complexes (Auble and Steggerda, 1999). Since NC2 and TBP encircle the DNA and do not interact in the absence of DNA, Mot1 likely disrupts the TBP:NC2 interaction as well.

Table 3. Distances of the cross-links detected between RecA1 and RecA2 subdomains of Mot1^{CTD} mapped on different structural models

Detected linkages		Euclidean C _α -C _α distance [Å]			Total number of detected cross links			
Residue 1	Residue 2	SsoRad54-like ('open')	DrRad54 ('closed')	ScChd1 ('semi-closed')	ADP·BeF _x	ATPγS	ADP	
	796	1013	16	22	20	1	1	1
	796	1200	25	17	16	1	1	0
	842	1055	58	52	52	0	1	0
A	864	1039	39	49	50	1	1	1
	1003	1013	12	11	10	1	0	1
	1003	1200	15	18	16	2	1	1
	1008	1200	12	14	12	2	0	1
B	864	1200	34	24	24	1	1	1
	919	1086	25	42	47	1	1	1
	865	1200	31	20	21	1	1	0
C	919	1051	63	22	43	1	0	0
	919	1055	57	19	36	2	2	0
	919	1060	51	25	36	1	0	0

Part A shows the cross links, which do not distinguish between the conformations. Part B and C list cross-links, for which the mapped distances were significantly different depending on the model used (i.e., <30 Å for one model and >30 Å for another). Eight of these cross-links (shown also in **Figure 6C**) were detected only in the presence of ADP·BeF_x and ATPγS and are listed in part C.

DOI: [10.7554/eLife.07432.017](https://doi.org/10.7554/eLife.07432.017)

Discussion

Swi2/Snf2-type ATPases remodel protein:DNA complexes to regulate the structure and epigenetic state of chromatin regions during transcription, DNA replication, and DNA repair. Mot1, apart from being an essential gene regulator, serves as an attractive model system for structural and mechanistic studies of Swi2/Snf2 enzymes. Here, we provide a pseudoatomic structure of the Swi2/Snf2 enzyme Mot1 bound to its protein:DNA substrate and a detailed structural framework for the interaction of Mot1 with the TBP:DNA:NC2 complex.

Swi2/Snf2 enzymes typically remodel protein:DNA complexes by disrupting the interface between the nucleic and protein partners of the target complex. ATP hydrolysis-dependent translocation of the Swi2/Snf2 ATPase domain could provide most if not all of the chemomechanical force, but a question is whether binding of the remodeler induces conformational changes in the target. Indeed, we find that the association of Mot1 with the TBP:DNA:NC2 complex results in some unexpected conformational changes that may have implications for understanding the ATP-dependent dissociation mechanism. Binding of Mot1 leads to subtle but consistent conformational changes between substrate proteins and DNA, which could prime the complex for ATP-dependent disruption. Although the interface between Mot1 and NC2 that we observe in the crystal structure of the Mot1^{NTP}:TBP:DNA:NC2 complex is arguably very small, the contact between Mot1's insertion domain and NC2 could help separate NC2's main TBP anchor helix *H5* from TBP and *H4* from DNA. In support of this, the very C-terminal unstructured region of NC2β following helix *H5* has been previously shown to be responsible for the repressive role of NC2 (Yeung *et al.*, 1994; Yeung *et al.*, 1997).

Additionally, compared to the state in the absence of Mot1, the conformation of the upstream DNA appears to be altered. Indeed, recent experiments have shown that Mot1:TBP:DNA and TBP:DNA:NC2 complexes are mobile and flexible due to an equilibrium between bent and unbent DNA states (Schluesche *et al.*, 2007; Moyle-Heyrman *et al.*, 2012). However, consistent with the observation that Mot1-induced dynamic DNA behavior in the TBP:DNA complex occurs also on DNA templates which are too short to directly contact the ATPase domain (Moyle-Heyrman *et al.*, 2012), we propose that even minimal Mot1-dependent conformational changes could have a critical impact on the TBP-TATA box interaction, especially as the severely bent TATA box itself might accelerate

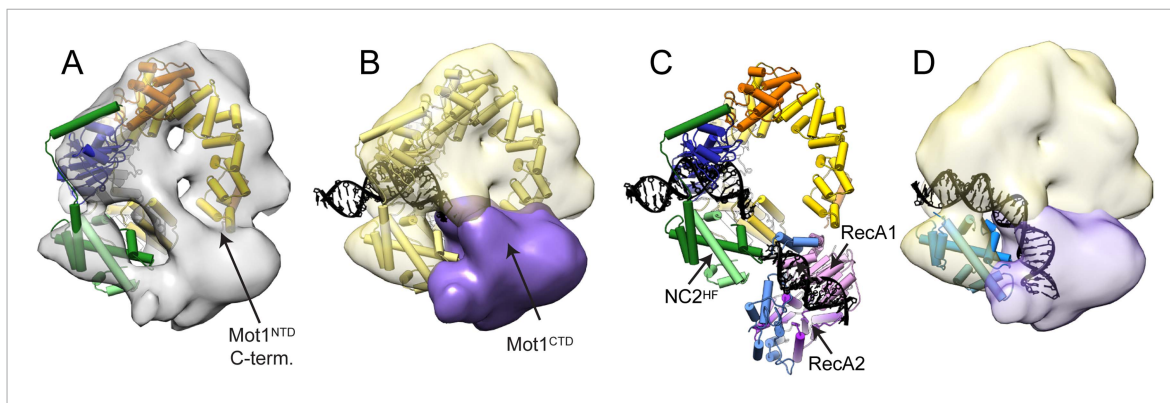


Figure 7. Pseudoatomic model for the Mot1:TBP:DNA:NC2 complex. Panels (A) and (B) show the Mot1^{NTD}:TBP:DNA:NC2 crystal structure rigid body docked into the negative stain EM map of the Mot1:TBP:DNA:NC2:ADP:BeF_x complex. (B) The density segment corresponding to Mot1^{CTD} (purple) is in a direct proximity to the C-terminal end of Mot1^{NTD} and to NC2^{HF}. The transparent yellow segment corresponds to the Mot1^{NTD}:TBP:NC2 module.

The TBP-bound promoter DNA fragment from the crystal structure is included (black). (C) Orientation of Mot1^{CTD} derived from the CX-MS data. For simplicity, one of the best-scoring models is shown. RecA1 (pink) and RecA2 (purple) correspond to the subdomains of a Swi2/Snf2 fold. Protrusions are indicated in blue. The DNA fragment bound to Mot1^{CTD} is modeled based on the SsoRad54-like:DNA crystal structure by superimposing via the RecA1 subdomain (Dürr *et al.*, 2005). (D) Overlay of the EM map segments from (B) and the crystal structure of NF-YB/NF-YC transcription factor (blue) bound to a DNA fragment (Nardini *et al.*, 2013) superimposed via the histone fold of NC2. Color coding for Mot1^{NTD}, TBP, and NC2 shown in (A) and (C) is the same as in Figure 4.

DOI: [10.7554/eLife.07432.018](https://doi.org/10.7554/eLife.07432.018)

The following figure supplements are available for figure 7:

Figure supplement 1. EM data.

DOI: [10.7554/eLife.07432.019](https://doi.org/10.7554/eLife.07432.019)

Figure supplement 2. Analysis of Mot1^{CTD} localization based on the CX-MS data.

DOI: [10.7554/eLife.07432.020](https://doi.org/10.7554/eLife.07432.020)

dissociation by acting as a ‘spring’ for rapid release of TBP (Tora and Timmers, 2010). This would be in line with, for example, DNase I footprinting experiments, which showed that Mot1 binding alters TBP’s TATA DNA protection pattern (Auble and Hahn, 1993; Darst *et al.*, 2001; Sprouse *et al.*, 2006), its ability to discriminate between classical and mutated TATA sequences, and why Mot1:TBP:DNA complexes can be formed by TBP mutants which are defective for TBP:DNA and Mot1:TBP complex formation (Gumbs *et al.*, 2003; Klejman *et al.*, 2005).

We also note that the conformation of TBP bound to DNA in the presence of Mot1 and NC2 is somewhat distinct from that of TBP bound to DNA alone and more similar to TBP bound to Mot1 alone (‘product’ complex, Figure 5—figure supplement 1D), although TBP remains in a rather similar conformation. The idea that Mot1 might directly influence TBP structure has been broadly discussed, although there has not yet been any direct evidence for it (Auble *et al.*, 1997; Adamkewicz *et al.*, 2000; Darst *et al.*, 2003; Gumbs *et al.*, 2003; Sprouse *et al.*, 2006; Auble, 2009). Therefore, inducing substantial conformational changes in the conserved TBP core domain seems to be rather unlikely. Nevertheless, according to our observations, Mot1 could still indirectly perturb TBP’s C-terminal stirrup, thereby affecting phenylalanine residues responsible for sharp DNA bending (Kim *et al.*, 1993).

NC2 prevents assembly of TBP with other general transcription factors (Meisterernst and Roeder, 1991; Inostroza *et al.*, 1992; Cang *et al.*, 1999; Kim *et al.*, 2008) but is retained on DNA in the absence of functional Mot1 *in vitro* and *in vivo* (Geisberg *et al.*, 2002; Schluesche *et al.*, 2007; Van Werven *et al.*, 2008; de Graaf *et al.*, 2010). While Mot1 forms a stable complex with DNA-bound TBP and NC2, it is fully capable of disrupting this complex in the presence of ATP. Thus, our data suggest that the TBP:DNA:NC2 complex is not only a *bona fide* but perhaps even preferential substrate for Mot1. It is possible that NC2 marks the TBP-containing complexes for Mot1-catalyzed disassembly, e.g., to prevent the formation of aberrant transcription preinitiation complexes on intragenic regions (Van Werven *et al.*, 2008; Spedale *et al.*, 2012; Koster *et al.*, 2014; Koster and Timmers, 2015). In this context, it is important to note that NC2, similarly to histones, has been shown to undergo phosphorylation, acetylation, methylation, and ubiquitination *in vivo* (Dephoure *et al.*, 2008;

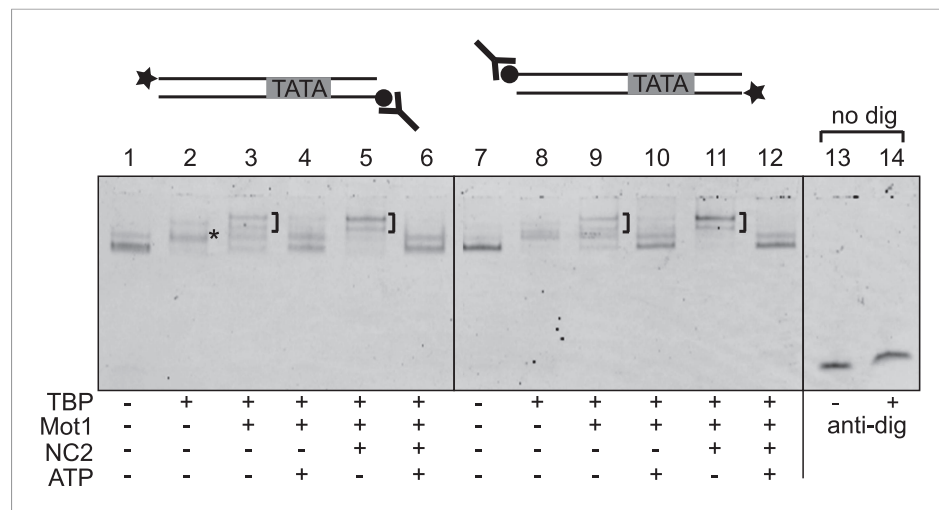


Figure 8. Mot1-mediated displacement of TBP and NC2 from end-blocked DNA templates. Electrophoretic mobility shift analysis of ATP-dependent disruption of Mot1:TBP:DNA complexes with and without NC2 as in **Figure 2**, but using DNA substrates that carry a digoxigenin label at one end (circle) and fluorescein for DNA detection at the other end (star). Reactions in lanes 13 and 14 were performed using DNA alone without digoxigenin modification, and demonstrate that the addition of digoxigenin antibody (Y-shape) had no effect on the mobility of unmodified DNA. Blocking of either end by the antibody did not result in a detectable decrease in TBP dissociation activity, suggesting that Mot1 does not translocate an intact TBP:NC2 clamp along DNA but locally disrupts the TBP:DNA:NC2 complex.

DOI: [10.7554/eLife.07432.021](https://doi.org/10.7554/eLife.07432.021)

Wang et al., 2008; Van Hoof et al., 2009; Huttlin et al., 2010; Kim et al., 2011; Alcolea et al., 2012; Wagner et al., 2012; Zhou et al., 2013; Guo et al., 2014; Sharma et al., 2014). Therefore, the impact of NC2 modifications on Mot1 recruitment and activity needs to be further investigated, especially given that the remodeling activity of Swi2/Snf2 family members can be controlled by post-translational modification of histone substrates or remodeler subunits themselves (*Clapier et al., 2002; Ferreira et al., 2007; Dutta et al., 2014*).

Importantly, the CX-MS analysis uncovered unanticipated interactions between Mot1^{CTD} and NC2. The position of Mot1^{CTD} relative to NC2^{HF} in our CX-MS- and EM-derived models is analogous to the association of a Swi2/Snf2 domain bound to superhelical location 2 (SHL2), i.e., in direct proximity to the H3/H4 histone pair slightly away from the dyad axis (*Dang and Bartholomew, 2007; Dechassa et al., 2012*). Notably, most of the cross-links between the Mot1^{CTD} and NC2^{HF} map to the protrusion region of the RecA2-like subdomain, the major family-specific insertion region of Swi2/Snf2 ATPases (*Flaus et al., 2006*). A general role for the Swi2/Snf2 protrusions in distorting local DNA structure has been proposed (*Hauk and Bowman, 2011*). For example, Snf2 has been suggested to disturb histone:DNA contacts by wedging the RecA2 lobe between DNA and protein substrates (*Dechassa et al., 2012*). In our model, the Swi2/Snf2 protrusions, especially from the RecA2 subdomain, are well positioned to directly affect DNA and NC2:DNA contacts. Therefore, the close proximity of the Mot1 Swi2/Snf2 domain to the NC2 histone fold reveals interesting parallels to the proposed interactions of nucleosome remodelers and histones (**Figure 9**), although more detailed structural investigation is necessary to elucidate the extent to which these architectures are conserved or distinct.

In summary, we provide here a first structural framework for the interaction of a Swi2/Snf2 ATPase in complex with its protein:DNA substrate. Our structural analyses suggest a two-step mechanism for the remodeling of TBP:DNA:NC2 by Mot1 that could be relevant for other remodelers that act on histone fold protein substrates. It seems plausible to reason that in the first step, TBP's and NC2's interaction with DNA is destabilized by Mot1 binding in an ATP-independent manner. ATP binding does not result in the disassembly of the complex. The formation of the Mot1^{NTD}:NC2 clamp ensures robust dependence on ATP hydrolysis, which triggers the final dissociation step, and which most probably occurs by very short-range translocation of the Swi2/Snf2 domain along the minor groove. Considering the relative orientation of Mot1^{CTD} and DNA in our model as well as the 3'-5' tracking

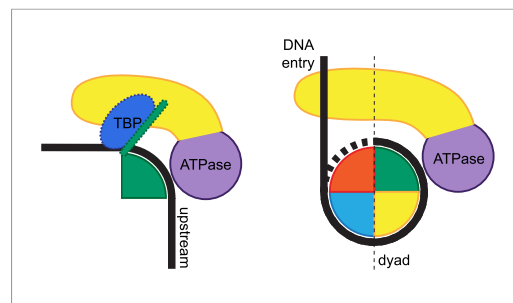


Figure 9. Remodeling of substrate protein:DNA complexes by Mot1 and comparison to the ISWI-type nucleosome remodeler. Left side: the binding of Mot1^{NTD} (yellow) induces destabilization of TBP:DNA and NC2:DNA interactions (TBP is shown in blue, NC2 is represented by a green shape). Right side: an ISWI-type Swi2/Snf2 remodeler bound to nucleosome according to current models (Dang and Bartholomew, 2007; Yamada et al., 2011; Hota et al., 2013). The DNA-binding domain (yellow) engages extranucleosomal DNA at the entry site. In both cases, the Swi2/Snf2 ATPase domains (purple) specifically recognize their histone fold: DNA substrates.

DOI: 10.7554/eLife.07432.022

direction shown for other Swi2/Snf2 enzymes (Whitehouse et al., 2003; Zofall et al., 2006), Mot1 may move along upstream DNA towards TBP, disrupting the TBP:promoter interaction.

Materials and methods

Protein expression and purification

N-terminally His₆-tagged full-length *Encephalitozoon cuniculi* Mot1 (1–1256) and Mot1^{NTD} (1–778) and N-terminally His₆-tagged full-length TBP (1–198) were expressed and purified as previously described (Wollmann et al., 2011). *E. coli* BL21 Rosetta(DE3) cells (Novagen, Germany) were used to co-express His₆-tagged full-length NC2 β (1–147) with the untagged full-length NC2 α (1–95). Initial purification of the NC2 α :NC2 β heterodimer was performed using Ni²⁺-NTA resin (Qiagen, Germany). Tobacco etch virus protease digestion was performed to cutoff the tag. Next, ion exchange chromatography using HiTrap SP HP column (GE Healthcare, Germany) connected to AEKTA purifier (GE Healthcare) was applied followed by gel filtration using S75 16/60 column (GE Healthcare) as the final step.

Selenomethionine labeling

Selenomethionine labeling in insect cells was performed for the N-terminally His₆-tagged Mot1^{NTD} construct. High 5 insect cell culture (Invitrogen, Germany) was adapted to Sf-900 II SFM medium (Gibco, Germany) by growing the cells from a starting concentration of 4·10⁵/ml for 4 days (27.5°C, 95 rpm). Subsequently, the cells were diluted to 1·10⁶/ml in 0.5 L of Sf-900 II SFM medium and infected 1:750 (vol/vol) with P2 virus. The culture was grown for 12 hr and centrifuged (800 rpm, 10 min). The cell pellet was resuspended in 0.5 L of Sf-900 II SFM medium supplied with 75 mg of L-cysteine (Sigma-Aldrich, Germany). After 4 hr of methionine depletion the cells were centrifuged and resuspended in 0.5 L of Sf-900 II SFM medium supplied with 75 mg of L-cysteine and 35 mg of L-selenomethionine (Acros, Germany). The expression was carried out for 48 hr (27.5°C, 95 rpm). The media were supplied with 1.4 μ g/ml gentamycin (Roth, Germany) and 10 mM L-glutamine (Gibco).

For the derivatization in *Escherichia coli* expression system, the plasmids were transformed into *E. coli* Rosetta B834 cells (Novagen, Germany) and grown in LB medium (37°C, 200 rpm). The expression cultures were grown in Selenomethionine Medium Base supplemented with Nutrient Mix (Molecular Dimensions, UK). Additionally, selenomethionine solution (Acros) at a final concentration of 42 μ g/ml was added to the sterile medium prior to inoculation. The media and selenomethionine solution were prepared according to the instruction supplied by the manufacturer. The cultures were grown until OD₆₀₀ reached 0.4 (160 rpm, 37°C). Next, the temperature was set to 18°C and the cultures were further grown until OD₆₀₀ \approx 0.7. The expression was induced with IPTG (Roth, 0.5 mM) and carried out overnight (18°C, 160 rpm). All of the used media were supplemented with appropriate antibiotics dependent on the resistance-coding expression plasmids. The applied protein purification protocols did not differ from the ones used for the purification of native proteins.

Electrophoretic mobility shift assays

Electrophoretic mobility shift assays (EMSAs) were performed essentially as previously described (Wollmann et al., 2011) using 47 bp oligonucleotide duplex probes labeled with fluorescein at the 5' end of one strand. For the EMSAs in Figure 2, the top strand DNA sequence was 5'–GGGTAC GGCCGGGCGCCCCGGATGGGGGGCTATAAAAGGGGGTGGGC–3'. Fluorescently labeled DNA (0.5 nM) was incubated for 20 min with TBP (20 nM) and Mot1 or Mot1^{Alatch} (30 nM) and with or without 30 nM NC2 as indicated. ATP (50 μ M) was then added for 5 min. Reactions were incubated at 25°C in 4% glycerol, 4 mM Tris–HCl (pH 8), 60 mM KCl, 5 mM MgCl₂, and 100 mg/ml bovine serum

albumin and were resolved on 6% non-denaturing gels. The gels were imaged using a Typhoon Trio phosphorimager as previously described (Wollmann *et al.*, 2011). DNA probes used for anti-digoxygenin conjugation (Figure 8) were 47 base pairs with the same sequence as above, but with either digoxigenin or fluorescein conjugated to the 5' end of either the top or bottom strand in each probe. EMSAs performed using the digoxigenin probes and anti-digoxygenin antibody (2.5 nM) were performed in the same way as described above except that reaction products were resolved on 5% gels to improve resolution. Anti-digoxygenin antibody was from Abcam (UK, 21H8).

Complex formation in gel filtration

DNA and single protein components were mixed and incubated in a stepwise manner at 4°C. TBP was first added to the TATA box-containing DNA in excess. This was followed by the addition of NC2 and Mot1/Mot1^{NTD}. Finally, the sample was centrifuged and loaded onto a S200 10/300 GL column connected to AEKTA purifier (GE Healthcare). 20 mM MES pH 6.5, 60 mM KCl, 5 mM MgCl₂ and 2 mM DTT or 20 mM HEPES pH 8.2, 60 mM KCl, 5 mM MgCl₂ and 2 mM DTT were used for the crystallization or EM and CX-MS analyses, respectively. Oligonucleotides were ordered from Biomers, Germany.

Crystallization, data collection, and structure determination

For the crystallization of the Mot1^{NTD}:TBP:DNA:NC2 complex, 24 double-stranded DNA (5'-AGTAAAGGGCTATAAAAGGGGGTGGC-3' top strand) was used. The peak gel filtration fractions were pooled, concentrated by ultrafiltration (Millipore, Germany), and centrifuged. The crystals were grown at 20°C for 7–14 days by hanging drop vapor diffusion technique. Best diffraction quality crystals were obtained by serial streak seeding from selenomethionine-derivatized proteins and grown in 0.2 M imidazole malate pH 5.1 and 9–16% PEG4000 condition. The crystals were flash-frozen in liquid nitrogen using original condition supplemented with 25% glycerol for cryoprotection. Diffraction data was collected at the European Synchrotron Radiation Facility (ID-29) at 100 K and $\lambda = 0.9794 \text{ \AA}$. The data were processed with XDS (Kabsch, 2010) in the space group C 1 2 1 ($a = 150.6 \text{ \AA}$, $b = 140.3 \text{ \AA}$, $c = 90.8 \text{ \AA}$, $\alpha = 90.0^\circ$, $\beta = 113.7^\circ$, $\gamma = 90.0^\circ$) with 60% solvent and one complex per asymmetric unit. The structure was successfully solved by molecular replacement with Phaser, part of the CCP4 software suite (McCoy *et al.*, 2007; Winn *et al.*, 2011). Homology model of the NC2 heterodimer was prepared using CHAINSAW (CCP4, Stein, 2008; Winn *et al.*, 2011). The structure was refined in BUSTER (v. 2.10.1) at 3.8 Å using TLS refinement strategy (Bricogne *et al.*, 2011) and manually rebuilt in Coot (Emsley *et al.*, 2010). Solvent flattening was performed with Parrot (CCP4, Cowtan, 2010; Winn *et al.*, 2011). B-factor sharpening and calculation of feature-enhanced $2F_o - F_c$ map was performed using PHENIX (Adams *et al.*, 2010; Afonine *et al.*, 2015). The histone fold region was characterized by relatively high B-factors and poor density and, therefore, the side chains of the residues NC2 α 15–89 and NC2 β 12–101 were omitted in the final model. The quality of the structure was evaluated with MolProbity (Davis *et al.*, 2007); 96%, 4%, and 0.0% of the residues were in Ramachandran favored, allowed, and outlier regions, respectively.

Negative stain EM

For the negative stain EM analysis of the Mot1:TBP:DNA:NC2 complex, 38 dsDNA was used (5'-CAGGCCGGGCGCCCCGGCATGGCGGCCTATAAAAGGGTC-3' top strand). The sample was supplied with 1 mM ADP·BeF_x. For the grid preparation sample was diluted to 25 µg/ml. The sample was applied to glow-discharged continuous carbon-coated grids. 5 µl of the sample was incubated for 1 min, blotted dry, washed twice with water, and finally fixed in a 1% (wt/vol) uranyl acetate solution. A total of 144 micrographs were recorded manually on a CM200 field emission gun transmission electron microscope (Philips, Netherlands) operated at 200 keV. Images were recorded on a 4k × 4k Gatan Ultrascan CCD camera using a defocus ranging from 0.5 to 1.5 µm and a dose of 25 e⁻/Å². The pixel size corresponded to 1.61 Å on the specimen level. Contrast-transfer function (CTF) determination and phase correction of the micrographs were performed using the TOM software package (Nickell *et al.*, 2005). From the corrected micrographs a total of 27,276 particles were selected using the 'boxer' tool from EMAN2 (Tang *et al.*, 2007). All subsequent image processing was carried out in XMIPP (Scheres *et al.*, 2008). The particles were normalized before further analysis by two-dimensional (2D) reference-free alignment and classification using the ML2D algorithm. Initial

reconstruction of a 3D volume from the particles was carried out using a reference-free approach using a sphere with the approximate particle diameter (10 nm) as an initial model for de novo ML3D alignment. Subsequently, ML3D classification was performed to sort out broken complexes or other non-particles, resulting in 8192 particles used for further refinement. The generated de novo model was filtered to 40 Å and used as an initial reference for iterative projection-matching refinement yielding the final reconstruction of the Mot1:TBP:DNA:NC2:ADP:BeF_x complex at a resolution of 22 Å, according to FSC (0.5 criterion) of two averages, each comprising 50% of the data. The resulting volume showed a good agreement with the previously RCT reconstructed map of Mot1, although more details were present. The map shows all features expected for the determined resolution, most pronounced in the C-shaped contour of the Mot1 protein itself. The resulting volume was furthermore assessed using different approaches (**Figure 7—figure supplement 1**).

Chemical cross-linking and enrichment of cross-linked peptides

For the CX-MS analysis of the Mot1:TBP:DNA:NC2 complex, 42 double-stranded DNA was used (5′-CAGTACGGCCGGGCGCCCGGCATGGCGGCCTATAAAAGGGTC-3′ top strand). The complex sample at 0.66 mg/ml was supplemented with 1 mM ATP_γS, 1 mM ADP, or 1 mM ADP:BeF_x (formed by mixing ADP, BeCl₂ and NaF in 1:1:4 molar ratio). An equimolar mixture of isotopically light (d0)- and heavy (d6)-labeled disulfosuccinimidyl glutarate (DSSG; Creative Molecules, Canada) was dissolved in H₂O at a concentration of 50 mM. 55 μg of protein complex were incubated with DSSG (0.32 mM final concentration) for 35 min at 30°C (1000 rpm). The reaction was quenched by adding 1 M Tris-HCl pH 8.0 to a final concentration of 100 mM, followed by incubation for further 15 min at 30°C (1000 rpm). The cross-linking efficiency was visualized by SDS-PAGE in combination with silver staining following standard protocols (**Figure 6—figure supplement 1**). Proteins were in the following digested using a standard in-solution protocol. In brief, proteins were denatured by adding two volumes of 8 M urea (Sigma-Aldrich). Cross-linked proteins were reduced with 5 mM final concentration tris(2-carboxyethyl)phosphine (TCEP, Thermo Scientific, Germany) for 45 min at 35°C and subsequently alkylated in the dark for 30 min at room temperature (10 mM iodoacetamide final concentration). Proteins were pre-digested for 2 hr with lysyl endopeptidase (LysC, Wako, Germany) at 35°C at an enzyme-substrate ratio of 1–50 (wt/wt). The protein solution was diluted with four volumes of 50 mM ammonium bicarbonate (ABC), and a second digest was performed overnight with trypsin (Promega, Germany, 1/50 [wt/wt] at 35°C, 1000 rpm). Peptides were acidified with 1% (vol/vol) trifluoroacetic acid (TFA, Sigma-Aldrich) and purified by solid-phase extraction using C18 cartridges (Sep-Pak, Waters, Germany). The desalted eluate was dried by vacuum centrifugation and reconstituted in 20 μl of size exclusion chromatography mobile phase (25% acetonitrile [ACN], 0.1% TFA). 15 μl hereof was injected into a GE Healthcare ÄKTAmicro chromatography system via autosampler. Peptides were separated on a Superdex Peptide PC 3.2/30 column (GE Healthcare) at a flow rate of 25 μl/min. 100 μl fractions were collected in a 96-well plate over a separation window of one column volume. The four fractions containing cross-linked peptides were dried to completeness and reconstituted in 2% ACN, 0.1% formic acid (FA).

Mass spectrometric analysis of cross-linked peptides and data analysis

Peptides sample were analyzed on an LC-MS/MS system using an UHPLC (EASY-nLC 1000) online coupled to an LTQ Orbitrap Elite (both Thermo Scientific) equipped with a standard nanoelectrospray source. A volume corresponding to an estimated 1 μg of peptide was injected onto a 15 cm × 0.050 mm I.D. reversed phase column packed with 2 μm C18 beads (Acclaim PepMap RSLC analytical column, Thermo Scientific). Peptides were separated using a 60 min gradient of solvent B (98% ACN, 0.1% FA) from 2% to 35% at a flow rate of 250 nl/min. Each sample was injected twice to improve identification of cross-linked peptides. The mass spectrometer was operated in data-dependent mode, selecting up to 10 precursors from a MS¹ scan (resolution = 120,000) in a mass range of 300–2000 m/z for rapid collision-induced dissociation (rCID). Singly and doubly charged precursors as well as precursors of unknown charge state were rejected for MS² selection. CID was performed for 10 ms using 35% normalized collision energy and an activation *q* of 0.25. Dynamic exclusion was activated with a repeat count of 1, exclusion duration 30 s at a list size of 500 and a mass window of ± 10 ppm. Ion target values were 1,000,000 (or maximum fill time of 10 ms) for the survey scan and 10,000 (or maximum fill time of 100 ms) for the MS² scan, respectively.

For data analysis, Thermo Xcalibur .RAW files were first converted to the open mzXML format using msconvert tool (ProteoWizard, *Kessner et al., 2008*). Cross-linked peptide candidates were extracted using the xQUEST (v. 2.1.1) pipeline including xProphet for FDR calculations (*Walzthoeni et al., 2012*). Standard settings were used. In brief, data were searched against a self-defined database containing Mot1, TBP, and NC2 proteins. Maximum number of missed cleavages (excluding the cross-linking site) = 2, peptide length = 4–45, enzyme = trypsin, fixed modifications = carbamidomethyl-Cys (57.02146 Da), variable modification = Met-oxidation (15.99491 Da), mass shift of the light cross-linker (96.02112937 Da), MS¹ tolerance = 10 ppm, MS² tolerance = 0.2 for common ions and 0.3 Da for cross-linked ions. The theoretical candidate spectra were scored according to their quality of the match and cross-linked candidates were filtered by a MS¹ mass tolerance of –5 to 5 ppm and a Δscore of ≥15% (indicating the relative score difference to the next ranked match). All spectra passing the filtering criteria were further manually validated. Identifications were only considered for the final result list in case both peptides had at least four bond cleavages in total or three adjacent ones and a minimum length of five amino acids. Full list of the detected cross-links can be found in [Table 2—source data 1](#).

Rigid body fitting into EM density map

The rigid body docking of Mot1^{NTD}:TBP:DNA:NC2 crystal structure was performed using *colores* applying a 10° sampling step size (*Chacón and Wriggers, 2002*). The search probe was down-filtered to 22 Å, and Laplacian filter (maximizing the fitting contrast) was applied. The DNA was omitted from the model, and the missing side chains of NC2^{HF} were included and set to most common rotamers. The fitting was performed for the correct and mirrored reconstruction and resulted in several fits of the Mot1^{NTD}:TBP:NC2 module. After manual inspection, two very similar solutions (for the rightful hand) were qualified as the correct solution. The other fits were nonsense fits resulted from template drifting, which often occurs at low resolution when the structure represents only a part of the density it is docked into (*Chacón and Wriggers, 2002*).

Mapping and scoring of the cross links

The set of Mot1^{CTD} orientations (n = 20,000) was generated using *RANCH*, part of the EOM package (*Petoukhov et al., 2012*) in a ‘compact’ mode, where Mot1^{NTD}:TBP:NC2 module was assumed to be flexibly linked to Mot1^{CTD} via the eight amino acid linker (residues 779–786, not present in the atomic models). Next, the models were displayed and the distances were measured using a standard script in PyMOL Molecular Graphics System (v. 1.5.0.4 Schrödinger, LLC). Finally, the models were scored according to the number of cross-links violating the 30 Å cutoff distance. For residues NC2α K61, K62, K92, and NC2β K27, which were not visible in the crystal structure (i.e., comprising short loop regions) but important for the analysis, the distances refer to the position which could be unambiguously modeled based on the crystal structure of NF-Y complex (PDB-ID 4AWL, *Nardini et al., 2013*). All reported distances between detected cross-linked lysines refer to the Euclidean C_α–C_α distances between the residues.

Figure preparation

The figures were prepared using UCSF Chimera package (*Pettersen et al., 2004*), PyMOL Molecular Graphics System (v. 1.5.0.4 Schrödinger, LLC) and OriginPro 8 G (OriginLab, Northampton, MA).

Accession NUMBERS

The coordinates and structure factors of the crystal structure were deposited in the Protein Data Bank under accession code 4WZS. The EM reconstruction map was deposited in the EMDB database under accession code 2828.

Acknowledgements

We thank Sebastian Eustermann for the discussion and Oana Mihalache for help with preparation of the grids, the Max-Planck Crystallization Facility (Martinsried) for crystallization trials and the synchrotron facilities ESRF (Grenoble), SLS (Villingen), and DESY-Petra III (Hamburg) for beam time and excellent on-site support. AB acknowledges support from the International Max Planck Research School for Molecular and Cellular Life Sciences.

Additional information

Funding

Funder	Grant reference	Author
Deutsche Forschungsgemeinschaft (DFG)	SFB 646	Karl-Peter Hopfner
European Research Council (ERC)	ATMMACHINE	Karl-Peter Hopfner
National Institutes of Health (NIH)	GM55763	David T Auble
Deutsche Forschungsgemeinschaft (DFG)	GRK1721	Friedrich Förster, Karl-Peter Hopfner

The funders had no role in study design, data collection and interpretation, or the decision to submit the work for publication.

Author contributions

AB, Acquisition of data, Analysis and interpretation of data, Drafting or revising the article; JMS, GS, PR-W, Acquisition of data, Analysis and interpretation of data; FF, Analysis and interpretation of data, Drafting or revising the article; DTA, Conception and design, Acquisition of data, Analysis and interpretation of data, Drafting or revising the article; K-PH, Conception and design, Analysis and interpretation of data, Drafting or revising the article

Author ORCIDs

Karl-Peter Hopfner,  <http://orcid.org/0000-0002-4528-8357>

Additional files

Major datasets

The following datasets were generated:

Author(s)	Year	Dataset title	Dataset ID and/or URL	Database, license, and accessibility information
Butryn A, Schuller JM, Stoehr G, Runge-Wollmann P, Förster F, Auble DT, Hopfner KP	2015	Structural basis for recognition and remodeling of the TBP: DNA:NC2 complex by Mot1	http://www.rcsb.org/pdb/explore/explore.do?structureId=4WZS	Publicly available at the Protein Data Bank (accession no. 4WZS).
Butryn A, Schuller JM, Stoehr G, Runge-Wollmann P, Förster F, Auble DT, Hopfner KP	2015	Structure of Mot1 in complex with TBP, NC2 and DNA	http://www.ebi.ac.uk/pdbe/entry/emdb/EMD-2828	Publicly available at EMDB (accession no. 2828).

References

- Adamkewicz JI, Mueller CG, Hansen KE, Prud'homme WA, Thorner J. 2000. Purification and enzymic properties of Mot1 ATPase, a regulator of basal transcription in the yeast *Saccharomyces cerevisiae*. *The Journal of Biological Chemistry* **275**:21158–21168. doi: [10.1074/jbc.M002639200](https://doi.org/10.1074/jbc.M002639200).
- Adams PD, Afonine PV, Bunkóczi G, Chen VB, Davis IW, Echols N, Headd JJ, Hung LW, Kapral GJ, Grosse-Kunstleve RW, McCoy AJ, Moriarty NW, Oeffner R, Read RJ, Richardson DC, Richardson JS, Terwilliger TC, Zwart PH. 2010. PHENIX: a comprehensive Python-based system for macromolecular structure solution. *Acta Crystallographica. Section D, Biological Crystallography* **66**:213–221. doi: [10.1107/S0907444909052925](https://doi.org/10.1107/S0907444909052925).
- Afonine PV, Moriarty NW, Mustyakimov M, Sobolec OV, Terwilliger TC, Turk D, Urzhumtsev A, Adams PD. 2015. FEM:feature-enhanced map. *Acta Crystallographica. Section D, Biological Crystallography* **71**:646–666. doi: [10.1107/S1399004714028132](https://doi.org/10.1107/S1399004714028132).
- Alcolea MP, Casado P, Rodriguez-Prados JC, Vanhaesebroeck B, Cutillas PR. 2012. Phosphoproteomic analysis of leukemia cells under basal and drug-treated conditions identifies markers of kinase pathway activation and mechanisms of resistance. *Molecular & Cellular Proteomics* **11**:453–466. doi: [10.1074/mcp.M112.017483](https://doi.org/10.1074/mcp.M112.017483).
- Andrau JC, Van Oevelen CJ, Van Teeffelen HA, Weil PA, Holstege FC, Timmers HT. 2002. Mot1p is essential for TBP recruitment to selected promoters during in vivo gene activation. *The EMBO Journal* **21**:5173–5183. doi: [10.1093/emboj/cdf485](https://doi.org/10.1093/emboj/cdf485).

- Auble DT. 2009. The dynamic personality of TATA-binding protein. *Trends in Biochemical Sciences* **34**:49–52. doi: [10.1016/j.tibs.2008.10.008](https://doi.org/10.1016/j.tibs.2008.10.008).
- Auble DT, Hahn S. 1993. An ATP-dependent inhibitor of TBP binding to DNA. *Genes & Development* **7**:844–856. doi: [10.1101/gad.7.5.844](https://doi.org/10.1101/gad.7.5.844).
- Auble DT, Hansen KE, Mueller CG, Lane WS, Thorner J, Hahn S. 1994. Mot1, a global repressor of RNA polymerase II transcription, inhibits TBP binding to DNA by an ATP-dependent mechanism. *Genes & Development* **8**:1920–1934. doi: [10.1101/gad.8.16.1920](https://doi.org/10.1101/gad.8.16.1920).
- Auble DT, Steggerda SM. 1999. Testing for DNA tracking by MOT1, a SWI2/SNF2 protein family member. *Molecular and Cellular Biology* **19**:412–423.
- Auble DT, Wang D, Post KW, Hahn S. 1997. Molecular analysis of the SWI2/SNF2 protein family member MOT1, an ATP-driven enzyme that dissociates TATA-binding protein from DNA. *Molecular and Cellular Biology* **17**:4842–4851.
- Bricogne G, Blanc E, Brandl M, Flensburg C, Keller P, Paciorek W, Roversi P, Sharff A, Smart OS, Vonrhein C, Womack TO. 2011. *BUSTER version 2.10.1*. Cambridge: United Kingdom Glob Phasing Ltd.
- Cang Y, Auble DT, Prelich G. 1999. A new regulatory domain on the TATA-binding protein. *The EMBO Journal* **18**:6662–6671. doi: [10.1093/emboj/18.23.6662](https://doi.org/10.1093/emboj/18.23.6662).
- Chacón P, Wriggers W. 2002. Multi-resolution contour-based fitting of macromolecular structures. *Journal of Molecular Biology* **317**:375–384. doi: [10.1006/jmbi.2001.5438](https://doi.org/10.1006/jmbi.2001.5438).
- Clapier CR, Cairns BR. 2009. The biology of chromatin remodeling complexes. *Annual Review of Biochemistry* **78**:273–304. doi: [10.1146/annurev.biochem.77.062706.153223](https://doi.org/10.1146/annurev.biochem.77.062706.153223).
- Clapier CR, Nightingale KP, Becker PB. 2002. A critical epitope for substrate recognition by the nucleosome remodeling ATPase ISWI. *Nucleic Acids Research* **30**:649–655. doi: [10.1093/nar/30.3.649](https://doi.org/10.1093/nar/30.3.649).
- Cowtan K. 2010. Recent developments in classical density modification. *Acta Crystallographica. Section D, Biological Crystallography* **66**:470–478. doi: [10.1107/S090744490903947X](https://doi.org/10.1107/S090744490903947X).
- Dang W, Bartholomew B. 2007. Domain architecture of the catalytic subunit in the ISW2-nucleosome complex. *Molecular and Cellular Biology* **27**:8306–8317. doi: [10.1128/MCB.01351-07](https://doi.org/10.1128/MCB.01351-07).
- Darst RP, Dasgupta A, Zhu C, Hsu JY, Vroom A, Muldrow T, Auble DT. 2003. Mot1 regulates the DNA binding activity of free TATA-binding protein in an ATP-dependent manner. *The Journal of Biological Chemistry* **278**:13216–13226. doi: [10.1074/jbc.M211445200](https://doi.org/10.1074/jbc.M211445200).
- Darst RP, Wang D, Auble DT. 2001. MOT1-catalyzed TBP-DNA disruption: uncoupling DNA conformational change and role of upstream DNA. *The EMBO Journal* **20**:2028–2040. doi: [10.1093/emboj/20.8.2028](https://doi.org/10.1093/emboj/20.8.2028).
- Dasgupta A, Darst RP, Martin KJ, Afshari CA, Auble DT. 2002. Mot1 activates and represses transcription by direct, ATPase-dependent mechanisms. *Proceedings of the National Academy of Sciences of USA* **99**:2666–2671. doi: [10.1073/pnas.052397899](https://doi.org/10.1073/pnas.052397899).
- Davis IW, Leaver-Fay A, Chen VB, Block JN, Kapral GJ, Wang X, Murray LW, Arendall WB III, Snoeyink J, Richardson JS, Richardson DC. 2007. MolProbity: all-atom contacts and structure validation for proteins and nucleic acids. *Nucleic Acids Research* **35**:W375–W383. doi: [10.1093/nar/gkm216](https://doi.org/10.1093/nar/gkm216).
- Dechassa ML, Hota SK, Sen P, Chatterjee N, Prasad P, Bartholomew B. 2012. Disparity in the DNA translocase domains of SWI/SNF and ISW2. *Nucleic Acids Research* **40**:4412–4421. doi: [10.1093/nar/gks007](https://doi.org/10.1093/nar/gks007).
- Dephoure N, Zhou C, Villén J, Beausoleil SA, Bakalarski CE, Elledge SJ, Gygi SP. 2008. A quantitative atlas of mitotic phosphorylation. *Proceedings of the National Academy of Sciences of USA* **105**:10762–10767. doi: [10.1073/pnas.0805139105](https://doi.org/10.1073/pnas.0805139105).
- Dürr H, Körner C, Müller M, Hickmann V, Hopfner KP. 2005. X-Ray structures of the *Sulfolobus solfataricus* SWI2/SNF2 ATPase core and its complex with DNA. *Cell* **121**:363–373. doi: [10.1016/j.cell.2005.03.026](https://doi.org/10.1016/j.cell.2005.03.026).
- Dutta A, Gogol M, Kim JH, Smolle M, Venkatesh S, Gilmore J, Florens L, Washburn MP, Workman JL. 2014. Swi/Snf dynamics on stress-responsive genes is governed by competitive bromodomain interactions. *Genes & Development* **28**:2314–2330. doi: [10.1101/gad.243584.114](https://doi.org/10.1101/gad.243584.114).
- Emsley P, Lohkamp B, Scott WG, Cowtan K. 2010. Features and development of Coot. *Acta Crystallographica. Section D, Biological Crystallography* **66**:486–501. doi: [10.1107/S0907444910007493](https://doi.org/10.1107/S0907444910007493).
- Ferreira H, Flaus A, Owen-Hughes T. 2007. Histone modifications influence the action of Snf2 family remodelling enzymes by different mechanisms. *Journal of Molecular Biology* **374**:563–579. doi: [10.1016/j.jmb.2007.09.059](https://doi.org/10.1016/j.jmb.2007.09.059).
- Flaus A, Martin DM, Barton GJ, Owen-Hughes T. 2006. Identification of multiple distinct Snf2 subfamilies with conserved structural motifs. *Nucleic Acids Research* **34**:2887–2905. doi: [10.1093/nar/gkl295](https://doi.org/10.1093/nar/gkl295).
- Gangaraju VK, Bartholomew B. 2007. Mechanisms of ATP dependent chromatin remodeling. *Mutation Research* **618**:3–17. doi: [10.1016/j.mrfmmm.2006.08.015](https://doi.org/10.1016/j.mrfmmm.2006.08.015).
- Geisberg JV, Moqtaderi Z, Kuras L, Struhl K. 2002. Mot1 associates with transcriptionally active promoters and inhibits association of NC2 in *Saccharomyces cerevisiae*. *Molecular and Cellular Biology* **22**:8122–8134. doi: [10.1128/MCB.22.23.8122-8134.2002](https://doi.org/10.1128/MCB.22.23.8122-8134.2002).
- de Graaf P, Mousson F, Geverts B, Scheer E, Tora L, Houtsmuller AB, Timmers HT. 2010. Chromatin interaction of TATA-binding protein is dynamically regulated in human cells. *Journal of Cell Science* **123**:2663–2671. doi: [10.1242/jcs.064097](https://doi.org/10.1242/jcs.064097).
- Grünwald M, Lazzaretti D, Bono F. 2013. Structural basis for the nuclear export activity of Importin13. *The EMBO Journal* **32**:899–913. doi: [10.1038/emboj.2013.29](https://doi.org/10.1038/emboj.2013.29).
- Gumbs OH, Campbell AM, Weil PA. 2003. High-affinity DNA binding by a Mot1p-TBP complex: implications for TAF-independent transcription. *The EMBO Journal* **22**:3131–3141. doi: [10.1093/emboj/cdg304](https://doi.org/10.1093/emboj/cdg304).

- Guo A**, Gu H, Zhou J, Mulhern D, Wang Y, Lee KA, Yang V, Aguiar M, Kornhauser J, Jia X, Ren J, Beausoleil SA, Silva JC, Vemulapalli V, Bedford MT, Comb MJ. 2014. Immunoaffinity enrichment and mass spectrometry analysis of protein methylation. *Molecular & Cellular Proteomics* **13**:372–387. doi: [10.1074/mcp.O113.027870](https://doi.org/10.1074/mcp.O113.027870).
- Hauk G**, Bowman GD. 2011. Structural insights into regulation and action of SWI2/SNF2 ATPases. *Current Opinion in Structural Biology* **21**:719–727. doi: [10.1016/j.sbi.2011.09.003](https://doi.org/10.1016/j.sbi.2011.09.003).
- Hauk G**, McKnight JN, Nodelman IM, Bowman GD. 2010. The chromodomains of the Chd1 chromatin remodeler regulate DNA access to the ATPase motor. *Molecular Cell* **39**:711–723. doi: [10.1016/j.molcel.2010.08.012](https://doi.org/10.1016/j.molcel.2010.08.012).
- Hota SK**, Bhardwaj SK, Deindl S, Lin YC, Zhuang X, Bartholomew B. 2013. Nucleosome mobilization by ISW2 requires the concerted action of the ATPase and SLIDE domains. *Nature Structural & Molecular Biology* **20**:222–229. doi: [10.1038/nsmb.2486](https://doi.org/10.1038/nsmb.2486).
- Hsu JY**, Juven-Gershon T, Marr MT II, Wright KJ, Tjian R, Kadonaga JT. 2008. TBP, Mot1, and NC2 establish a regulatory circuit that controls DPE-dependent versus TATA-dependent transcription. *Genes & Development* **22**:2353–2358. doi: [10.1101/gad.1681808](https://doi.org/10.1101/gad.1681808).
- Huber EM**, Scharf DH, Hortschansky P, Groll M, Brakhage AA. 2012. DNA minor groove sensing and widening by the CCAAT-binding complex. *Structure* **20**:1757–1768. doi: [10.1016/j.str.2012.07.012](https://doi.org/10.1016/j.str.2012.07.012).
- Huttlin EL**, Jedrychowski MP, Elias JE, Goswami T, Rad R, Beausoleil SA, Villén J, Haas W, Sowa ME, Gygi SP. 2010. A tissue-specific atlas of mouse protein phosphorylation and expression. *Cell* **143**:1174–1189. doi: [10.1016/j.cell.2010.12.001](https://doi.org/10.1016/j.cell.2010.12.001).
- Inostroza JA**, Mermelstein FH, Ha I, Lane WS, Reinberg D. 1992. Dr1, a TATA-binding phosphoprotein and inhibitor of class II gene transcription. *Cell* **70**:477–489. doi: [10.1016/0092-8674\(92\)90172-9](https://doi.org/10.1016/0092-8674(92)90172-9).
- Kabsch W**. 2010. XDS. *Acta Crystallographica. Section D, Biological Crystallography* **66**:125–132. doi: [10.1107/S0907444909047337](https://doi.org/10.1107/S0907444909047337).
- Kamada K**, Shu F, Chen H, Malik S, Stelzer G, Roeder RG, Meisterernst M, Burley SK. 2001. Crystal structure of negative cofactor 2 recognizing the TBP-DNA transcription complex. *Cell* **106**:71–81. doi: [10.1016/S0092-8674\(01\)00417-2](https://doi.org/10.1016/S0092-8674(01)00417-2).
- Kessner D**, Chambers M, Burke R, Agus D, Mallick P. 2008. ProteoWizard: open source software for rapid proteomics tools development. *Bioinformatics* **24**:2534–2536. doi: [10.1093/bioinformatics/btn323](https://doi.org/10.1093/bioinformatics/btn323).
- Kim JL**, Nikolov DB, Burley SK. 1993. Co-crystal structure of TBP recognizing the minor groove of a TATA element. *Nature* **365**:520–527. doi: [10.1038/365520a0](https://doi.org/10.1038/365520a0).
- Kim W**, Bennett EJ, Huttlin EL, Guo A, Li J, Possemato A, Sowa ME, Rad R, Rush J, Comb MJ, Harper JW, Gygi SP. 2011. Systematic and quantitative assessment of the ubiquitin-modified proteome. *Molecular Cell* **44**:325–340. doi: [10.1016/j.molcel.2011.08.025](https://doi.org/10.1016/j.molcel.2011.08.025).
- Kim Y**, Ebright YW, Goodman AR, Reinberg D, Ebright RH. 2008. Nonradioactive, ultrasensitive site-specific protein-protein photocrosslinking: interactions of alpha-helix 2 of TATA-binding protein with general transcription factor TFIIA and transcriptional repressor NC2. *Nucleic Acids Research* **36**:6143–6154. doi: [10.1093/nar/gkn612](https://doi.org/10.1093/nar/gkn612).
- Klejman MP**, Pereira LA, van Zeeburg HJ, Gilfillan S, Meisterernst M, Timmers HT. 2004. NC2alpha interacts with BTAF1 and stimulates its ATP-dependent association with TATA-binding protein. *Molecular and Cellular Biology* **24**:10072–10082. doi: [10.1128/MCB.24.22.10072-10082.2004](https://doi.org/10.1128/MCB.24.22.10072-10082.2004).
- Klejman MP**, Zhao X, van Schaik FM, Herr W, Timmers HT. 2005. Mutational analysis of BTAF1-TBP interaction: BTAF1 can rescue DNA-binding defective TBP mutants. *Nucleic Acids Research* **33**:5426–5436. doi: [10.1093/nar/gki850](https://doi.org/10.1093/nar/gki850).
- Koster MJ**, Timmers HT. 2015. Regulation of anti-sense transcription by Mot1p and NC2 via removal of TATA-binding protein (TBP) from the 3'-end of genes. *Nucleic Acids Research* **43**:143–152. doi: [10.1093/nar/gku1263](https://doi.org/10.1093/nar/gku1263).
- Koster MJ**, Yildirim AD, Weil PA, Holstege FC, Timmers HT. 2014. Suppression of intragenic transcription requires the MOT1 and NC2 regulators of TATA-binding protein. *Nucleic Acids Research* **42**:4220–4229. doi: [10.1093/nar/gkt1398](https://doi.org/10.1093/nar/gkt1398).
- Krissinel E**, Henrick K. 2007. Inference of macromolecular assemblies from crystalline state. *Journal of Molecular Biology* **372**:774–797. doi: [10.1016/j.jmb.2007.05.022](https://doi.org/10.1016/j.jmb.2007.05.022).
- Lewis R**, Dürr H, Hopfner KP, Michaelis J. 2008. Conformational changes of a Swi2/Snf2 ATPase during its mechano-chemical cycle. *Nucleic Acids Research* **36**:1881–1890. doi: [10.1093/nar/gkn040](https://doi.org/10.1093/nar/gkn040).
- Luger K**, Mäder AW, Richmond RK, Sargent DF, Richmond TJ. 1997. Crystal structure of the nucleosome core particle at 2.8 Å resolution. *Nature* **389**:251–260. doi: [10.1038/38444](https://doi.org/10.1038/38444).
- McCoy AJ**, Grosse-Kunstleve RW, Adams PD, Winn MD, Storoni LC, Read RJ. 2007. Phaser crystallographic software. *Journal of Applied Crystallography* **40**:658–674. doi: [10.1107/S0021889807021206](https://doi.org/10.1107/S0021889807021206).
- Meisterernst M**, Roeder RG. 1991. Family of proteins that interact with TFIID and regulate promoter activity. *Cell* **67**:557–567. doi: [10.1016/0092-8674\(91\)90530-C](https://doi.org/10.1016/0092-8674(91)90530-C).
- Moyle-Heyrman G**, Viswanathan R, Widom J, Auble DT. 2012. Two-step mechanism for modifier of transcription 1 (Mot1) enzyme-catalyzed displacement of TATA-binding protein (TBP) from DNA. *The Journal of Biological Chemistry* **287**:9002–9012. doi: [10.1074/jbc.M111.333484](https://doi.org/10.1074/jbc.M111.333484).
- Nardini M**, Gnesutta N, Donati G, Gatta R, Forni C, Fossati A, Vornrhein C, Moras D, Romier C, Bolognesi M, Mantovani R. 2013. Sequence-specific transcription factor NF-Y displays histone-like DNA binding and H2B-like ubiquitination. *Cell* **152**:132–143. doi: [10.1016/j.cell.2012.11.047](https://doi.org/10.1016/j.cell.2012.11.047).
- Nguyen VQ**, Ranjan A, Stengel F, Wei D, Aebersold R, Wu C, Leschziner AE. 2013. Molecular architecture of the ATP-dependent chromatin-remodeling complex SWR1. *Cell* **54**:1220–1231. doi: [10.1016/j.cell.2013.08.018](https://doi.org/10.1016/j.cell.2013.08.018).
- Nickell S**, Förster F, Linaroudis A, Net DW, Beck F, Hegerl R, Baumeister W, Plitzko JM. 2005. TOM software toolbox: acquisition and analysis for electron tomography. *Journal of Structural Biology* **149**:227–234. doi: [10.1016/j.jsb.2004.10.006](https://doi.org/10.1016/j.jsb.2004.10.006).

- Pereira LA**, Klejman MP, Ruhlmann C, Kavelaars F, Oulad-Abdelghani M, Timmers HT, Schultz P. 2004. Molecular architecture of the basal transcription factor B-TFIID. *The Journal of Biological Chemistry* **279**:21802–21807. doi: [10.1074/jbc.M313519200](https://doi.org/10.1074/jbc.M313519200).
- Petoukhov MV**, Franke D, Shkumatov AV, Tria G, Kikhney AG, Gajda M, Gorba C, Mertens HD, Konarev PV, Svergun DI. 2012. New developments in the ATSAS program package for small-angle scattering data analysis. *Journal of Applied Crystallography* **45**:342–350. doi: [10.1107/S0021889812007662](https://doi.org/10.1107/S0021889812007662).
- Petterson EF**, Goddard TD, Huang CC, Couch GS, Greenblatt DM, Meng EC, Ferrin TE. 2004. UCSF Chimera—a visualization system for exploratory research and analysis. *Journal of Computational Chemistry* **25**:1605–1612. doi: [10.1002/jcc.20084](https://doi.org/10.1002/jcc.20084).
- Politis A**, Stengel F, Hall Z, Hernández H, Leitner A, Walzthoeni T, Robinson CV, Aebersold R. 2014. A mass spectrometry-based hybrid method for structural modeling of protein complexes. *Nature Methods* **11**:403–406. doi: [10.1038/nmeth.2841](https://doi.org/10.1038/nmeth.2841).
- Ponomarev MA**, Timofeev VP, Levitsky DI. 1995. The difference between ADP-beryllium fluoride and ADP-aluminium fluoride complexes of the spin-labeled myosin subfragment 1. *FEBS Letters* **371**:261–263. doi: [10.1016/0014-5793\(95\)00898-J](https://doi.org/10.1016/0014-5793(95)00898-J).
- Saha A**, Wittmeyer J, Cairns BR. 2002. Chromatin remodeling by RSC involves ATP-dependent DNA translocation. *Genes & Development* **16**:2120–2134. doi: [10.1101/gad.995002](https://doi.org/10.1101/gad.995002).
- Scheres SH**, Núñez-Ramírez R, Sorzano CO, Carazo JM, Marabini R. 2008. Image processing for electron microscopy single-particle analysis using XMIPP. *Nature Protocols* **3**:977–990. doi: [10.1038/nprot.2008.62](https://doi.org/10.1038/nprot.2008.62).
- Schluesche P**, Stelzer G, Piaia E, Lamb DC, Meisterernst M. 2007. NC2 mobilizes TBP on core promoter TATA boxes. *Nature Structural & Molecular Biology* **14**:1196–1201. doi: [10.1038/nsmb1328](https://doi.org/10.1038/nsmb1328).
- Sengoku T**, Nureki O, Nakamura A, Kobayashi S, Yokoyama S. 2006. Structural basis for RNA unwinding by the DEAD-box protein Drosophila Vasa. *Cell* **125**:287–300. doi: [10.1016/j.cell.2006.01.054](https://doi.org/10.1016/j.cell.2006.01.054).
- Sharma A**, Jenkins KR, Héroux A, Bowman GD. 2011. Crystal structure of the chromodomain helicase DNA-binding protein 1 (Chd1) DNA-binding domain in complex with DNA. *The Journal of Biological Chemistry* **286**:42099–42104. doi: [10.1074/jbc.C111.294462](https://doi.org/10.1074/jbc.C111.294462).
- Sharma K**, D'Souza RC, Tyanova S, Schaab C, Wiśniewski JR, Cox J, Mann M. 2014. Ultradeep human phosphoproteome reveals a distinct regulatory nature of Tyr and Ser/Thr-based signaling. *Cell Reports* **8**:1583–1594. doi: [10.1016/j.celrep.2014.07.036](https://doi.org/10.1016/j.celrep.2014.07.036).
- Shaw G**, Gan J, Zhou YN, Zhi H, Subburaman P, Zhang R, Joachimiak A, Jin DJ, Ji X. 2008. Structure of RapA, a Swi2/Snf2 protein that recycles RNA polymerase during transcription. *Structure* **16**:1417–1427. doi: [10.1016/j.str.2008.06.012](https://doi.org/10.1016/j.str.2008.06.012).
- Spedale G**, Meddens CA, Koster MJ, Ko CW, van Hooff SR, Holstege FC, Timmers HT, Pijnappel WW. 2012. Tight cooperation between Mot1p and NC2 β in regulating genome-wide transcription, repression of transcription following heat shock induction and genetic interaction with SAGA. *Nucleic Acids Research* **40**:996–1008. doi: [10.1093/nar/gkr784](https://doi.org/10.1093/nar/gkr784).
- Sprouse RO**, Brenowitz M, Auble DT. 2006. Swi2/Snf2-related ATPase Mot1 drives displacement of TATA-binding protein by gripping DNA. *The EMBO Journal* **25**:1492–1504. doi: [10.1038/sj.emboj.7601050](https://doi.org/10.1038/sj.emboj.7601050).
- Stein N**. 2008. CHAINSAW: a program for mutating pdb files used as templates in molecular replacement. *Journal of Applied Crystallography* **41**:641–643. doi: [10.1107/S0021889808006985](https://doi.org/10.1107/S0021889808006985).
- Tang G**, Peng L, Baldwin PR, Mann DS, Jiang W, Rees I, Ludtke SJ. 2007. EMAN2: an extensible image processing suite for electron microscopy. *Journal of Structural Biology* **157**:38–46. doi: [10.1016/j.jsb.2006.05.009](https://doi.org/10.1016/j.jsb.2006.05.009).
- Thomä NH**, Czyzewski BK, Alexeev AA, Mazin AV, Kowalczykowski SC, Pavletich NP. 2005. Structure of the SWI2/SNF2 chromatin-remodeling domain of eukaryotic Rad54. *Nature Structural & Molecular Biology* **12**:350–356. doi: [10.1038/nsmb919](https://doi.org/10.1038/nsmb919).
- Tora L**, Timmers HT. 2010. The TATA box regulates TATA-binding protein (TBP) dynamics in vivo. *Trends in Biochemical Sciences* **35**:309–314. doi: [10.1016/j.tibs.2010.01.007](https://doi.org/10.1016/j.tibs.2010.01.007).
- Tosi A**, Haas C, Herzog F, Gilmozzi A, Berninghausen O, Ungewickell C, Gerhold CB, Lakomek K, Aebersold R, Beckmann R, Hopfner KP. 2013. Structure and subunit topology of the INO80 chromatin remodeler and its nucleosome complex. *Cell* **154**:1207–1219. doi: [10.1016/j.cell.2013.08.016](https://doi.org/10.1016/j.cell.2013.08.016).
- Van Hoof D**, Muñoz J, Braam SR, Pinkse MW, Linding R, Heck AJ, Mummery CL, Krijgsveld J. 2009. Phosphorylation dynamics during early differentiation of human embryonic stem cells. *Cell Stem Cell* **5**:214–226. doi: [10.1016/j.stem.2009.05.021](https://doi.org/10.1016/j.stem.2009.05.021).
- Van Werven FJ**, van Bakel H, van Teeffelen HA, Altelaar AF, Koerkamp MG, Heck AJ, Holstege FC, Timmers HT. 2008. Cooperative action of NC2 and Mot1p to regulate TATA-binding protein function across the genome. *Genes & Development* **22**:2359–2369. doi: [10.1101/gad.1682308](https://doi.org/10.1101/gad.1682308).
- Wagner SA**, Beli P, Weinert BT, Schölz C, Kelstrup CD, Young C, Nielsen ML, Olsen JV, Brakebusch C, Choudhary C. 2012. Proteomic analyses reveal divergent ubiquitylation site patterns in murine tissues. *Molecular & Cellular Proteomics* **12**:1578–1585. doi: [10.1074/mcp.M112.017905](https://doi.org/10.1074/mcp.M112.017905).
- Walzthoeni T**, Claassen M, Leitner A, Herzog F, Bohn S, Förster F, Beck M, Aebersold R. 2012. False discovery rate estimation for cross-linked peptides identified by mass spectrometry. *Nature Methods* **9**:901–903. doi: [10.1038/nmeth.2103](https://doi.org/10.1038/nmeth.2103).
- Wang Z**, Gucek M, Hart GW. 2008. Cross-talk between GlcNAcylation and phosphorylation: site-specific phosphorylation dynamics in response to globally elevated O-GlcNAc. *Proceedings of the National Academy of Sciences of USA* **105**:13793–13798. doi: [10.1073/pnas.0806216105](https://doi.org/10.1073/pnas.0806216105).

- Whitehouse I**, Stockdale C, Flaus A, Szczelkun MD, Owen-Hughes T. 2003. Evidence for DNA translocation by the ISWI chromatin-remodeling enzyme. *Molecular and Cellular Biology* **23**:1935–1945. doi: [10.1128/MCB.23.6.1935-1945.2003](https://doi.org/10.1128/MCB.23.6.1935-1945.2003).
- Winn MD**, Ballard CC, Cowtan KD, Dodson EJ, Emsley P, Evans PR, Keegan RM, Krissinel EB, Leslie AG, McCoy A, McNicholas SJ, Murshudov GN, Pannu NS, Potterton EA, Powell HR, Read RJ, Vagin A, Wilson KS. 2011. Overview of the CCP4 suite and current developments. *Acta Crystallographica. Section D, Biological Crystallography* **67**:235–242. doi: [10.1107/S0907444910045749](https://doi.org/10.1107/S0907444910045749).
- Wollmann P**, Cui S, Viswanathan R, Berninghausen O, Wells MN, Moldt M, Witte G, Butryn A, Wendler P, Beckmann R, Auble DT, Hopfner KP. 2011. Structure and mechanism of the Swi2/Snf2 remodeler Mot1 in complex with its substrate TBP. *Nature* **475**:403–407. doi: [10.1038/nature10215](https://doi.org/10.1038/nature10215).
- Wriggers W**. 2010. Using Situs for the integration of multi-resolution structures. *Biophysical Reviews* **2**:21–27. doi: [10.1007/s12551-009-0026-3](https://doi.org/10.1007/s12551-009-0026-3).
- Yamada K**, Frouws TD, Angst B, Fitzgerald DJ, DeLuca C, Schimmele K, Sargent DF, Richmond TJ. 2011. Structure and mechanism of the chromatin remodelling factor ISW1a. *Nature* **472**:448–453. doi: [10.1038/nature09947](https://doi.org/10.1038/nature09947).
- Yeung K**, Kim S, Reinberg D. 1997. Functional dissection of a human Dr1-DRAP1 repressor complex. *Molecular and Cellular Biology* **17**:36–45.
- Yeung KC**, Inostroza JA, Mermelstein FH, Kannabiran C, Reinberg D. 1994. Structure-function analysis of the TBP-binding protein Dr1 reveals a mechanism for repression of class II gene transcription. *Genes & Development* **8**:2097–2109. doi: [10.1101/gad.8.17.2097](https://doi.org/10.1101/gad.8.17.2097).
- Zentner GE**, Henikoff S. 2013. Mot1 redistributes TBP from TATA-containing to TATA-less promoters. *Molecular and Cellular Biology* **33**:4996–5004. doi: [10.1128/MCB.01218-13](https://doi.org/10.1128/MCB.01218-13).
- Zhou H**, Di Palma S, Preisinger C, Peng M, Polat AN, Heck AJ, Mohammed S. 2013. Toward a comprehensive characterization of a human cancer cell phosphoproteome. *Journal of Proteome Research* **12**:260–271. doi: [10.1021/pr300630k](https://doi.org/10.1021/pr300630k).
- Zofall M**, Persinger J, Kassabov SR, Bartholomew B. 2006. Chromatin remodeling by ISW2 and SWI/SNF requires DNA translocation inside the nucleosome. *Nature Structural & Molecular Biology* **13**:339–346. doi: [10.1038/nsmb1071](https://doi.org/10.1038/nsmb1071).